Structure-activity relationships for binding of 4-substituted triazole-phenols to macrophage migration inhibitory factor (MIF)

Xiao, Zhangping; Fokkens, Marieke; Chen, Deng; Kok, Tjie; Proietti, Giordano; Van Merkerk, Ronald; Poelarends, Gerrit J.; Dekker, Frank J.

Published in:
European Journal of Medicinal Chemistry

DOI:
10.1016/j.ejmech.2019.111849

Document Version
Publisher's PDF, also known as Version of record

Publication date:
2020

European Journal of Medicinal Chemistry 186 (2020) 111849

Contents lists available at ScienceDirect

European Journal of Medicinal Chemistry

journal homepage: http://www.elsevier.com/locate/ejmech

Research paper

Structure-activity relationships for binding of 4-substituted triazole-phenols to macrophage migration inhibitory factor (MIF)

Zhangping Xiao [a], Marieke Fokkens [a], Deng Chen [a], Tjie Kok [a, b], Giordano Proietti [a], Ronald van Merkerk [a], Gerrit J. Poelarends [a], Frank J. Dekker [a, *]

[a] Chemical and Pharmaceutical Biology, Groningen Research Institute of Pharmacy (GRIP), University of Groningen, Groningen, the Netherlands
[b] Faculty of Biotechnology, University of Surabaya, Surabaya, Indonesia

ARTICLE INFO

Article history:
Received 16 July 2019
Received in revised form
18 October 2019
Accepted 3 November 2019
Available online 11 November 2019

Keywords:
Microphage migration inhibitory factor (MIF)
Transition metals
Triazole-phenols
Tautomerase activity
Clonogenic assay

ABSTRACT

Macrophage migration inhibitory factor (MIF) is a versatile protein that plays a role in inflammation, autoimmune diseases and cancers. Development of novel inhibitors will enable further exploration of MIF as a drug target. In this study, we investigated structure-activity relationships of MIF inhibitors using a MIF tautomerase activity assay to measure binding. Importantly, we notified that transition metals such as copper (II) and zinc (II) interfere with the MIF tautomerase activity under the assay conditions applied. EDTA was added to the assay buffer to avoid interference of residual heavy metals with tautomerase activity measurements. Using these assay conditions the structure-activity relationships for MIF binding of a series of triazole-phenols was explored. The most potent inhibitors in this series provided activities in the low micromolar range. Enzyme kinetic analysis indicates competitive binding that proved reversible. Binding to the enzyme was confirmed using a microscale thermophoresis (MST) assay. Molecular modelling was used to rationalize the observed structure-activity relationships. The most potent inhibitor **2d** inhibited proliferation of A549 cells in a clonogenic assay. In addition, **2d** attenuated MIF induced ERK phosphorylation in A549 cells. Altogether, this study provides insights in the structure-activity relationships for MIF binding of triazole-phenols and further validates this class of compounds as MIF binding agents in cell-based studies.

1. Introduction

Macrophage migration inhibitory factor (MIF) was discovered in 1966 by Bloom and Bennett as a cytokine that is implicated in the inhibition of macrophage motility [1]. Subsequently, MIF was also discovered to function as a hormone, a chemokine and as a molecular chaperone. Thus, MIF proved to be involved in various physiological and pathological processes [2–4]. Genetic deregulation of MIF (such as overexpression) has been implicated in many inflammatory and immune diseases in humans, such as diabetes, atherosclerosis and rheumatoid arthritis [5]. In addition, mounting evidence supports a role of MIF in tumorigenesis and progression [6]. Its key roles in health and disease raised interest in development of small molecule MIF modulators as potential therapeutics.

Many MIF functions are mediated by protein-protein interactions with membrane receptors. The cluster of differentiation 74 (CD74) receptor is the best characterized membrane receptor for MIF [7]. Recently, another membrane protein CD44 was reported as an integral component of the CD74 receptor complexthat proved to be essential for MIF signal transduction [8]. By forming a complex with CD74 and CD44, MIF triggers activation of the mitogen activated protein kinase (MAPK) pathway. Activation of this pathway is associated with MIF mediated oncogenesis and inflammation. MIF functions in inflammation and immune cell chemotaxis are also mediated by interactions with chemokine receptors such as CXCR2 and CXCR4 [4]. Besides extracellular functions, MIF is known to bind to intracellular protein targets such as Jun-activated domain-binding protein 1 (JAB1), which results in slowing down JAB1 mediated cell growth [9]. Therefore, development of molecules to interfere with MIF protein-protein interaction has emerged as an attractive strategy to block MIF signaling.

Prior evidence indicates that treatment with anti-MIF antibodies or small molecule MIF modulators enables disruption of MIF mediated functions [10]. Besides discovering a statistically significant up-regulation of MIF concentration in the blood of septic

* Corresponding author.
E-mail address: f.j.dekker@rug.nl (F.J. Dekker).

https://doi.org/10.1016/j.ejmech.2019.111849

patients, Calandra *et al*. reported that an anti-MIF antibody can protect TNFα-deficient mice from fulminant septic shock [11]. Neutralization of MIF with anti-MIF antibodies provied to be beneficial in autoimmune encephalomyelitis [12], endotoxic shock [13] and even cancer [14]. From the perspective of drug discovery, development of small molecule MIF binders has advantages compared to the development of antibodies [15,16]. Many small molecule MIF binders have been discovered, but only a few of them have been tested for their biological activity [17–19]. Progression along this line is needed to shed light on the utility of MIF binders as a potential novel strategy for management of inflammatory diseases.

Normally, MIF exists in a homotrimeric form in which each monomer contains 115 amino acids and has a molecular mass of 12.4 kDa [20]. Apart from its functions in protein-protein interactions, the MIF trimer also harbors keto-enol tautomerase activity. There are three tautomerase active sites in the MIF homotrimer, each located at the interface between two monomers, in which the residue Pro1 has a key role in catalysis [21]. Although, D-dopachrome and 4-hydroxyphenylpyruvate (4-HPP) were identified as substrates for the keto-enol tautomerase activity of MIF, the physiological role of this activity remains elusive. Recent findings indicate that Tyr36, Lys66 and Asn109, which are located on the surface surrounding the tautomerase active site pocket of MIF, are involved in activation of CD74 [22]. Besides, there is also a thiol-protein oxidoreductase (TPOR) active site located at the center of the enzyme, which is conferred by its Cys^{57}-Ala-Leu-Cys^{60} (CALC) motif [23]. Peptides containing the CALC region were reported to retain some biochemical properties of the full-length MIF protein [24]. The structural correlations between its enzymatic activity and its physiological functions provide opportunities to develop small molecule inhibitors of the enzymatic activity that also modulate the physiological functions in which MIF is involved.

Although, the MIF tautomerase activity shows no direct correlation with its biological functions, the pocket that harbors this enzymatic activity has been employed for development of inhibitors that should ultimately interfere with MIF protein-protein interactions [25–27]. Inhibitors include the mostly investigated dopachrome analogue **ISO-1**, inhibitor Orita-**13** and others (Fig. 1) [28–31]. Importantly, many previously described inhibitors have a non-reversible binding or a slow tight binding mode, [26], which obscures estimation of the equilibrium binding constants. Also direct measurement of the binding of compounds to the enzyme active site proved to be important to gain a realistic insight in the binding capacities of compounds that interfere with MIF tautomerase activity [32]. Recently, the Jorgensen group reported a series of competitive inhibitors of MIF tautomerase activity with a biaryltriazole structure for which they confirmed reversibility of binding. The K_i value of the most potent compound, Jorgensen-**3bb** ((Fig. 1), is 57 nM [33–35]. An interesting feature in their inhibitor collection is that adding a fluorine at the *ortho*-position of the phenolic hydroxyl group strongly favors inhibition. The highest potency was observed upon substitution on the triazole 4-position with a quinoline. However, this provides molecules with almost exclusively sp^2-hybridized atoms and consequently a very flat molecular structure. This limits water solubility and potentially inhibitor selectivity. The availability of structural information for binding of this class of inhibitors to MIF provides a basis to explore the structure-activity relationships (SAR) further.

Here we describe a SAR study for binding of the biaryltriazole-type of inhibitors to MIF. Using the triazole-phenol unit as a core, we have explored alternatives for the quinoline functionality in the triazole 4-position in order to find inhibitors with a less planar structure. Firstly, we identified the interference of transition metals such as copper(II) or zinc(II) with MIF tautomerase activity, followed by optimizing the assay through addition of ethylenediaminetetraacetic acid (EDTA) to the assay buffer. Subsequently, we investigated a compound collection of 27 triazole-phenols that was assembled using the copper catalyzed alkyne to azide cycloaddition (CuAAC) reaction as a key step. Using this approach, we were able to identify novel triazole-phenols that reversibly inhibit MIF tautomerase activity and also provide activity on the cellular level.

2. Results and discussion

2.1. MIF tautomerase activity assay optimization

Recombinant human MIF was expressed and purified following methods published previously by our group [30] and others. [32] The MIF tautomerase activity assay using 4-HPP as a substrate (Fig. 2A) was established using previously described assay conditions [30]. To determine the IC_{50}, the compounds were diluted from DMSO (20 μL) with water or water with 20 mM EDTA (10 μL) into a a 96 well plate. Subsequently, the dilutions were pre-incubated with the MIF enzyme solution (760 nM, 170 μL) for 15 min. The assay was started by mixing 50 μL of the inhibitor enzyme pre-incubation mixture with 50 μL of an aqeous 4-HPP (1.0 mM) solution. This provides a reaction mixture with 380 nM of the enzyme, 0.5 mM 4-HPP and various concentration of the inhibitor. In the positive control, MIF was incubated with a blanc DMSO dilution as a vehicle control before adding the 4-HPP substrate. In the negative control, the substrate was mixed with a blanc DMSO dilution in absence of MIF as an enzyme. In the negative control, the UV absorbance did not change over time, which was set to 0%, whereas the positive control was set to 100%.

To test the stability of MIF, 3 samples from the same batch of enzyme were stored at 4 °C for 1, 12 and 25 days, respectively, after being taken from the −80 °C freezer. Different storage times provide the same tautomerase activity levels (Fig. S1). In addition, unfolding temperatures of fresh enzyme and enzyme stored for 2 weeks in at 4 °C were determined by nanoDSF to be 77.9 °C and 78.9 °C (Fig. S1). These results together show that MIF is stable upon prolonged storage at −80 °C or 4 °C.

During our studies we noticed that irreproducible results were obtained from inhibitors synthesized using the CuAAC "click

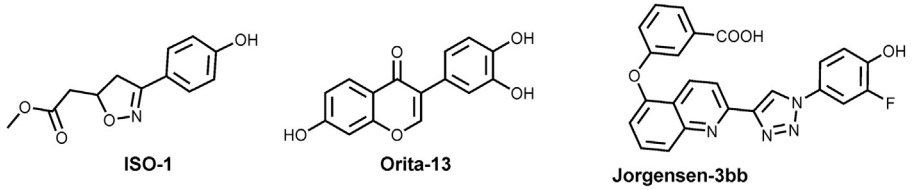

Fig. 1. Reported inhibitors of MIF. **ISO-1** is developed in 2002 by Al-Abed *et al*. and it is one of the most investigated inhibitors of MIF [28]. Orita-13 was found in 2001 by a structure-based computer-assisted search. Its K_i value was reported to be 38 nM [29]. Jorgensen-**3bb** is one of the most potent inhibitors of MIF reported to date with a K_i value of 57 nM [34].

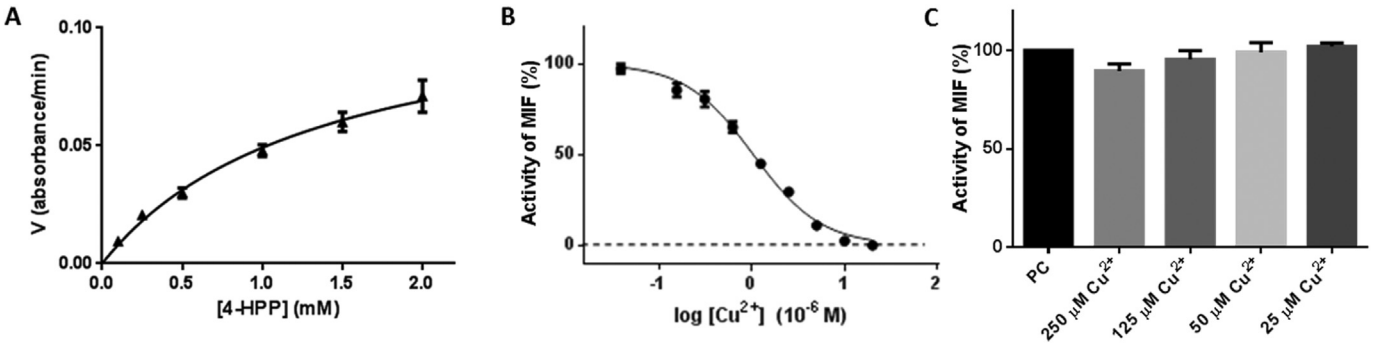

Fig. 2. MIF tautomerase activity using 4-HPP as a substrate and effect of copper(II) on MIF tautomerase activity. A) MIF catalyzed conversion of 4-HPP. B) Concentration dependent inhibition of MIF tautomerase activity by copper(II). C) Residual tautomerase activity of MIF in presence of 0.5 mM EDTA and different concentrations of copper(II).

reaction". This raised the idea that transition metals such as copper could influence the MIF tautomerase activity assay that we employed in our studies. To our surprise, we found that copper(II) inhibits MIF tautomerase activity with an IC_{50} of 1.0 μM (Fig. 2B). Expanding on this finding we also found that zinc(II) inhibits MIF tautomerase activity with an IC_{50} of 1.0 μM (Fig. S3). This indicates that the observed inhibition does not depend on the redox potential of the transition metal but rather suggests a role for the metal ion as Lewis acid. These observations imply that presence of (traces of) transition metals could contribute to irregularities in MIF tautomerase inhibition assays [36].

Subsequently, we investigated the inhibition of MIF tautomerase activity by copper(II) further. In the regular assays, we apply MIF with a C-terminal His-tag. To test the influence of the His-tag, we used MIF without His-tag and found that the tautomerase activity of His-tag free MIF was also completely blocked in presence of 20 μM copper(II) (Fig. S4). In addition, we found that copper(II) also blocked the activity of a related enzyme, 4-oxalocrotonate tautomerase (4-OT), in a Michael addition reaction (Fig. S4) [37]. In the literature, it has been reported that the copper(II)-containing protein ceruloplasmin (CP) can suppress MIF enzymatic activity, [38], which is in line with our findings here. Altogether, these findings indicate that the transition metals copper(II) and zinc(II) can interfere with the 4-HPP tautomerization reaction catalyzed by MIF under the assay conditions applied in this study.

We adjusted the assay conditions to prevent interference of transition metals with MIF tautomerase enzyme activity in inhibitor binding studies. Including ethylenediaminetetraacetic acid (EDTA) in the assay buffer proved to be an effective strategy to prevent interference of copper(II) with the MIF tautomerase activity. Our results indicate that 125 μM copper(II) has no effect on 4-HPP tautomerization by MIF if 0.5 mM EDTA is added to the assay buffer (Fig. 2C). Addition of EDTA did not influence the Km value for 4-HPP conversion as both conditions provided a Km of 1.1 mM in the Michealis-Menten enzyme kinetics (Fig. S2). Based on these findings we included 0.5 mM EDTA in the MIF tautomerase assay buffer in our studies. This is particularly important for activity measurements of 4-(1,2,3-triazole)phenols, as studied here, because their synthesis requires significant amounts of copper, which could result in copper pollution of the final products.

We note that inhibition of MIF tautomerase activity by transition metals is the first time reported here, but that EDTA has already been used before in the assay buffer in MIF inhibitor development [29,39]. However, other studies, including those using CuAAC for inhibitor synthesis, did not apply EDTA in the assay buffer [34,35]. Here we provide a rationale to include EDTA in the assay buffer in cases where the presence of traces of transition metals in the final products can be expected.

2.2. Synthesis

A focused compound collection of 4-(1,2,3-triazole)phenol derivatives was obtained by coupling 4-azidophenol to various terminal alkynes using CuAAC (Scheme 1). In this study, the CuAAC reaction was performed by addition of a catalytic amount of $CuSO_4$ and sodium ascorbate in water to the alkyne and azide substrates dissolved in methanol. The reaction was allowed to proceed at room temperature or 60 °C for 12 h [40]. The terminal alkyne precursors for compounds of group A were prepared using propiolic acid as a key intermediate. Different amines were coupled to propiolic acid through a N,N′-Dicyclohexylcarbodiimide (DCC) mediated amidation. The subsequent step provided the final products in overall isolated yields between 30% and 86%. Compounds of group B were synthesized by coupling various aliphatic terminal alkynes to 4-azidophenol at room temperature to provide a series of 4-(1,2,3-triazole)phenol derivatives. For this series the isolated yields varied between 12% and 96%. Compounds of group C were synthesized using 2-propargylamine as key intermediate. Different carboxylic acids were coupled to propargylamine using DCC mediated amidation to provide substituted terminal alkynes that were subjected to the "click" reaction. These two subsequent reactions were conducted at room temperature with isolated yields between 15% and 98%. The variability of the yields could be attributed to the low solubility of several products in combination with the filtration in the final step of the synthesis.

2.3. Enzyme inhibition study

The focused compound collection was screened for inhibition of MIF tautomerase activity by an assay employing 4-HPP as a substrate. The assay conditions, as described above, include 0.5 mM EDTA to avoid interference of residual copper(II) with the tautomerase activity. The inhibitors were screened for MIF binding by measurement of the residual MIF tautomerase activity in presence of 50 μM of the respective inhibitor. MIF tautomerase inhibitors **ISO-1** and Jorgensen-**2b** were tested as a reference to literature values (Table 1). These inhibitors reduced the activity of MIF with percentages of 20% and 90% respectively at 50 μM, which is in line with their reported potency for MIF inhibition in literature [34].

Screening of the residual enzyme activity upon preincubation with 50 μM of the respective inhibitor provided clear structure-activity relationships for the three groups of 4-(1,2,3-triazole) phenol inhibitors as shown in Fig. 3. For compounds of group A the residual enzyme activity is around 75% of the positive control for all inhibitors, which indicates a potency similar to **ISO-1** without a clear structure-activity dependence. For group B the residual enzyme activity varies between 90% and 10% of the positive control,

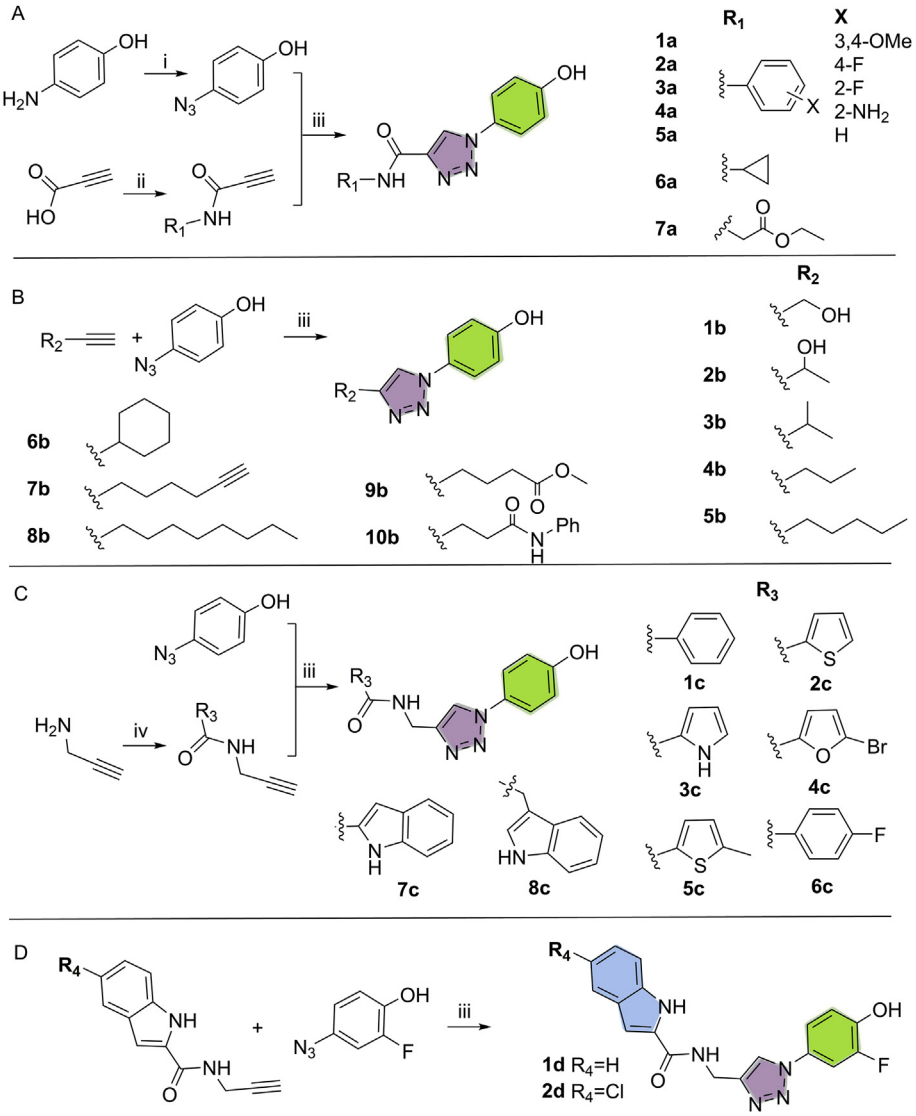

Scheme 1. Synthesis of MIF inhibitors in four main groups. Group A represents compounds with propiolic acid as key building block. Compounds of group B were synthesized using various aliphatic terminal alkynes. Compounds of group C contain propargylamine as key precursor. Compounds of group D take advantage of ortho-fluor substitution of the phenol for enhancing potency. Reagents and conditions: i. a) $NaNO_2$, HCl, H_2O, rt, 2h; b) NaN_3, rt,1h, 99%; ii. DCC, CH_3CN, rt, 2h, 95%; iii. $CuSO_4$ (0.1 eq), sodium ascorbate (0.2 eq), MeOH, rt, overnight, 12–90%; iv. DCC, CH_3CN, rt, 2h; v. Pd, H_2, rt, 4h, EtOH, 99%.

thus indicating a clear structure-activity dependence. Extending the 4-substitution of the 4-(1,2,3-triazole)phenol scaffold from propyl to pentyl and 5-hexynyl reduces the residual enzyme activity from 90% to 10% of the control, whereas octyl substitution provides increased residual enzyme activity. This indicates that an aliphatic tail with 5 or 6 carbon atoms is optimal in this series of inhibitors. The structure-activity relationships for the compounds in group C are less clear with residual enzyme activities between 40 and 10% of the control with compound **7c** as the most active one in this series.

All the compounds that inhibited MIF tautomerase activity by more than 50% of the positive control were subjected for IC_{50} determination. The IC_{50} values are shown in Table 1. K_i values are calculated by the Cheng-Prusoff equation: $K_i = IC_{50}/(1+[S]/K_M)$ [41] in which $K_M = 1.1$ mM. The K_i value of **ISO-1** was measured to be 44 ± 4.9 μM, which is in line with values reported in literature [30,36]. To further confirm the validity of our assays and to enable direct comparison, inhibitor Jorgensen-**2b** and **3b** were synthesized according to literature [42]. Using Jorgensen-**2b** we investigated the effect of addition of EDTA to the assay buffer on the IC_{50} and K_i values in the MIF inhibition assay. For Jorgensen-**2b**, a K_i of 5.0 ± 0.6 μM was determined in presence of 0.5 mM EDTA, whereas a K_i value of 2.9 ± 0.3 μM was determined in absence of 0.5 mM EDTA. This demonstrates that EDTA can influence the Ki values to a certain extend but that the observed differences are limited to less than a two-fold change in potency. K_i value of Jorgensen-**3b** was determined to be 0.42 ± 0.03 μM with 0.5 mM EDTA present. The K_i values observed in our assay are in line with the K_i of 8.8 and 0.59 μM for Jorgensen-**2b** and **3b**, respectively, reported before by Jorgensen [42].

Compounds in group A were not subjected to IC_{50} determinations due to a lack of inhibitory potency at concentrations of 50 μM. Group B provided two inhibitors with potencies in the low micromolar range. Compounds **5b** and **7b** had a K_i of 6.9 ± 0.3 μM and 6.5 ± 0.8 μM, respectively. The clear activity dependence on the length of the aliphatic tail indicates a role for lipophilic interactions in binding. For group C, inhibitors with variant monocyclic aromatic groups exhibit K_i values ranging from

Table 1
Inhibition of MIF tautomerase activity by 4-substituted triazole phenols.

	Comp.	R_1, R_2, R_3 or R_4	%residual activity[a]	IC_{50} (μM)	K_i (μM)
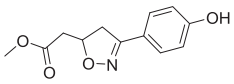	**ISO-1**	–	–	64 ± 7.1	44 ± 4.9
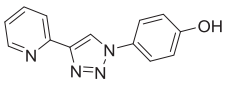	Jorgensen -**2b**	–	–	7.2 ± 0.9	5.0 ± 0.6
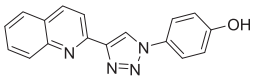	Jorgensen -**3b**	–	–	0.64 ± 0.05	0.44 ± 0.03
Group **A**	**1a**	3,4-OMe-phenyl	77%	–	–
	2a	4-F-phenyl	74%	–	–
	3a	2-F-phenyl	80%	–	–
	4a	2-amine-phenyl	77%	–	–
	5a	phenyl	71%	–	–
	6a	cyclopropyl	74%	–	–
	7a	2-ethoxy-2-oxoethyl	81%	–	–
Group **B**	**1b**	hydroxymethyl	91%	–	–
	2b	1-hydroxyethyl	73%	–	–
	3b	isopropyl	62%	–	–
	4b	propyl	50%	–	–
	5b	pentyl	–	10 ± 0.5	6.9 ± 0.3
	6b	cyclohexyl	–	26 ± 2.2	17 ± 1.5
	7b	5-hexynyl	–	9.5 ± 1.1	6.5 ± 0.8
	8b	octyl	53%	–	–
	9b	4-methoxy-4-oxobutyl	–	33 ± 2.0	23 ± 1.4
	10b	3-oxo-3-(phenylamino)propyl	–	47 ± 5.0	32 ± 3.4
Group **C**	**1c**	phenyl	–	33 ± 1.4	23 ± 1.0
	2c	thiophen-2-yl	–	41 ± 4.0	28 ± 2.7
	3c	1H-pyrrol-2-yl	–	43 ± 4.2	30 ± 2.9
	4c	5-bromofuran-2-yl	–	38 ± 4.1	26 ± 2.8
	5c	5-methylthiophen-2-yl	–	28 ± 2.0	19 ± 1.4
	6c	4-F-phenyl	–	53 ± 3.0	36 ± 2.0
	7c	1H-indol-2-yl	–	10 ± 0.7	6.9 ± 0.5
	8c	(1H-indol-3-yl)methyl	–	62 ± 4.0	43 ± 2.8
Group **D**	**1d**	H	–	4.8 ± 0.5	3.3 ± 0.3
	2d	Cl	–	1.4 ± 0.3	0.96 ± 0.2

[a] Residual MIF tautomerase activity in presence of 50 μM inhibitor.

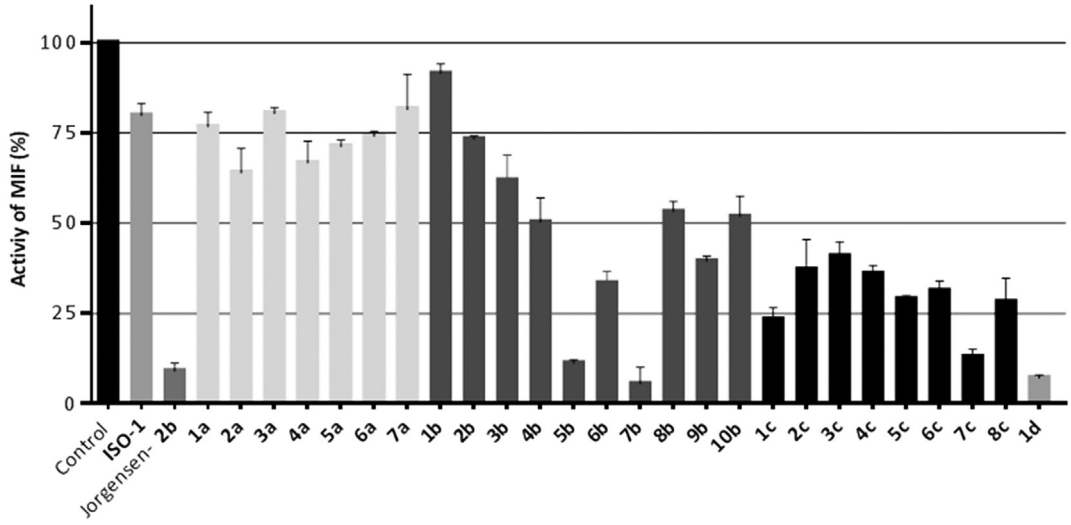

Fig. 3. Screening of the inhibitory potency of the triazole-phenol collection at 50 μM inhibitor concentration. The enzyme activity in absence of inhibitor was set to 100%. Data are presented as mean ± standard deviation (n = 3).

19 to 35 μM. However, the bycyclic indole functionality provided stronger inhibition with a K_i value of 6.9 ± 0.5 μM for **7c**. This could be due to both stacking and/or lipophilic interactions between the indole functionality of **7c** and MIF. Extending the single carbon atom spacer between the triazole and the indole in **7c** to a two-carbon atom spacer in **8c** caused a loss of potency with a K_i of 43 ± 2.8 μM, which indicates a clear structure dependence of the activity.

2.4. Inhibitor optimization and enzyme kinetic study

To further improve the inhibitory potency of the inhibitors identified against MIF, we substituted the phenolic *ortho*-position with a fluorine [34]. Therefore, two new inhibitors were synthesized as shown in Scheme 1D. The resulting compound **1d** provided a K_i of 3.2 ± 0.3 μM, which is two times enhanced compared to its equivalent without fluorine **7c** (Fig. 4A). This proves again that an ortho-fluoro substitution is a favorable modification for triazole-phenol MIF inhibitors. By substitution of the 5-position of the indole in **1d** with chlorine, inhibitor **2d** was obtained, which proved to me more potent with a K_i of 0.96 ± 0.2 μM. The solubility of **1d** and **2d** were respectively 24 ± 0.19 μg/mL (41.41 ± 0.51 μM) and 10.8 ± 0.10 μg/mL (28.01 ± 0.26 μM) in pH 7.4 PBS buffer as measured by the shake-flask method (Fig. S10). Both **1d** and **2d** have significantly improved aqueous solubility compared to inhibitor Jorgensen-**3b**, which is 2.2 μg/mL [34]. This demonstrates that reducing the planar character of inhibitors indeed improved water solubility. We note, however, that **2d** did not dissolve completely at concentrations of 50 μM and higher, which prohibits measuring full inhibition in the enzyme inhibition study.

To investigate the mechanism of inhibition and to avoid artefacts as described previously [25], the binding behavior of inhibitor **1d** was characterized further. A pre-incubation and dilution assay was performed to study reversibility of binding for **1d** to MIF. Towards this aim, MIF was pre-incubated with 83 μM of **1d** for 10 min before 100-fold dilution and testing of the residual enzyme activity. Upon pre-incubation with **1d** the MIF tautomerase activity could be fully recovered as compared to the positive control without inhibitor (Fig. 4B). This indicates reversible binding for **1d** to MIF.

The influence of inhibitor **1d** on the enzyme kinetics of MIF-catalyzed conversion of 4-HPP was analyzed (Fig. 4C, 4D). In presence of 2 or 5 μM **1d** the K_m increases from 1.14 to 1.60 and 1.95 μM respectively, whereas the V_{max} remains constant between 0.24 and 0.29 (absorbance/min) compared to 0.27 for the control (Table 2). Thus, the enzyme kinetics demonstrate that **1d** is a competitive inhibitor, which is consistent with previous reports for MIF inhibition by inhibitors with a triazole-phenol core [34]. Similar results were obtained for **2d** as shown in the supporting information.

2.5. Binding affinity study

To confirm binding of **1d** to MIF, we performed a microscale thermophoresis (MST) assay. MST is a newly emerging technology for analysis of binding to proteins. This technology exploits the ligand-induced changes in the molecular movement of fluorescently labeled proteins in a temperature gradient [43]. We determined the thermophoresis shift upon titration of different concentration of **1d** to 50 nM MIF. The K_D value was determined from the changes in thermal shifts upon titration of **1d**, which provides an sigmoidal curve from which the binding affinity (K_D) was calculated to be 3.63 μM. Thus, the K_D observed in the MST assay is comparable to the K_i value of 3.2 μM calculated from the enzyme kinetic experiments (Fig. 5). Altogether, we conclude that the 4-(1,2,3-triazole)phenol inhibitor **1d** binds reversibly to MIF with a potency in the low micromolar range.

Table 2
Enzyme kinetic parameters for inhibition of MIF by **1d**.

1d (μM)	K_m^{app} (mM)	V_{max}^{app} (absorbance/min)
0	1.14 ± 0.17	0.27 ± 0.02
1	1.60 ± 0.24	0.29 ± 0.02
2.5	1.95 ± 0.33	0.24 ± 0.02

The p-values show that the slopes are significantly non-zero (n = 3, p-value < 0.05).

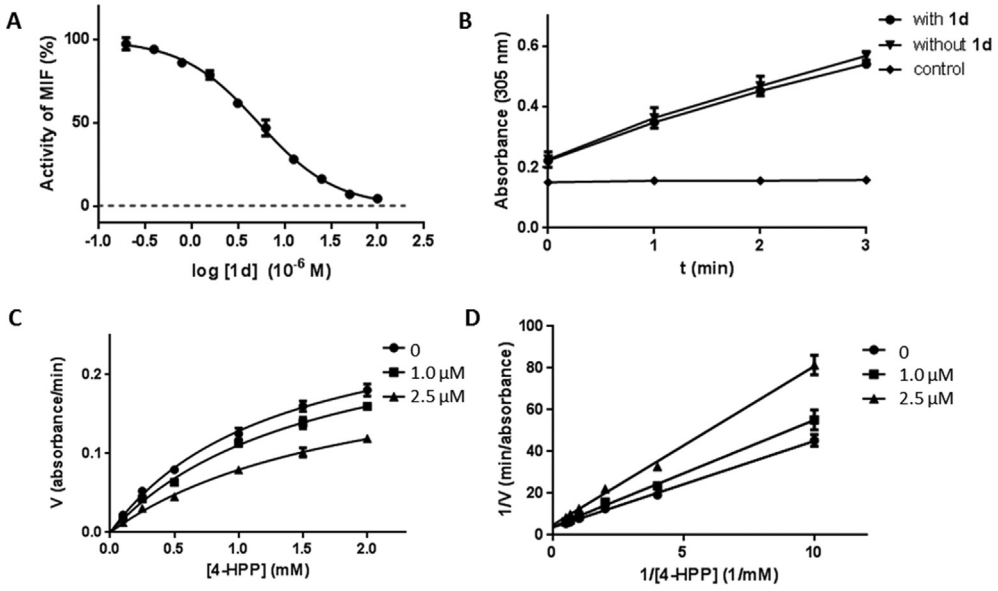

Fig. 4. Inhibition of MIF tautomerase activity by **1d**. A) Dose-response curve for inhibition of MIF tautomerase activity by **1d**. B) Pre-incubation and dilution assay of **1d** and MIF. After 10 min pre-incubation at 83 μM **1d** for 10 min the MIF solution was diluted 100-fold and employed for 4-HHP conversion. In the control group no enzyme was added. C) Michaelis-Menten plots of MIF activity at concentration of 0, 1.0 and 2.5 μM of inhibitor **1d**. D) Lineweaver-Burk plots of MIF at concentration of 0, 1.0 and 2.5 μM of **1d** (n is 3 for all results shown in this figure.).

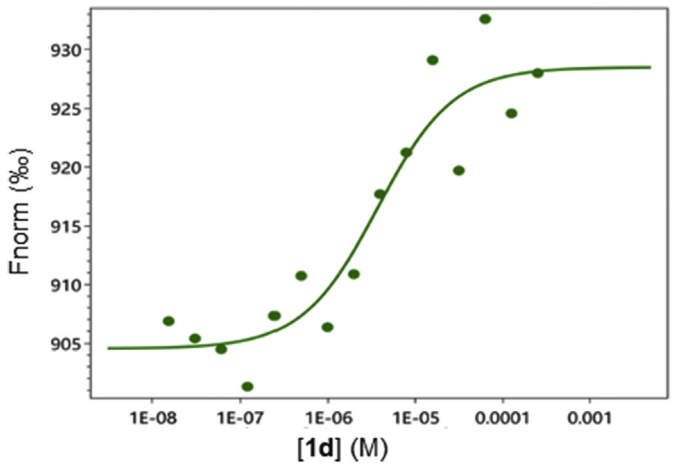

Fig. 5. Microscale thermophoresis measurements of the binding affinity of **1d** for MIF. Fnorm (Normalized fluorescence) = Fhot/Fcold. n = 3.

2.6. Molecular modeling

Docking studies were performed to rationalize the structure-activity relationships observed for MIF inhibition. Structural information for the MIF interaction of the analogous biaryltriazoles was used as a basis for molecular modeling (PDB code:4wrb and 5hvs) [34]. Modelling was performed using the software Discovery Studio 3.0. The compounds were docked into the crystal structure of MIF and energy minimized. The highest scoring poses were analyzed and compared with reference inhibitor Jorgensen-**3bb** [34]. The 2-fluoro-4-(1,2,3-triazole)phenol part of **1d** occupies the same position as observed in Jorgensen-**3bb** (Fig. 6A, 6B, 6C). A main difference is that the quinolone in Jorgensen-**3bb** occupies a position different from the indole 2-carboxamide functionality in **1d**. The difference in potency could originate from the loss of stacking interactions between the quinoline ring and residues Pro33 and Lys32 that convey a high potency to Jorgensen-**3bb**. Instead, **1d** has a hydrogen bond with Lys32 and a hydrophobic interaction with Ile64. Although **1d** does not reach the same potency as reported for Jorgensen-**3bb**, the interactions observed in the modelling appear to be useful, because they enable targeting of a different part of the binding pocket.

The structure-activity relationship was further rationalized by investigating details from docking poses of **1d**, **7c** and **3c**. A main difference between **1d** and **7c** is formation of a hydrogen bond between the fluoro and residue Asn97 in **1d**, which is not present in **7c**. The extra hydrogen bond can contribute to the two-times enhanced potency of **1d** compared to **7c**. Comparison was also made between **7c** with the indole 2-carboxamide that provided a K_i of 6.7 μM and **3c** with a pyrrole 2-carboxamide that provided a K_i of 29 μM (Fig. 6D, 6E). The 4-fold change in potency between **3c** and **7c** could be attributed to additional hydrophobic interaction with Ile64 in **7c**.

2.7. A549 cell colony formation assay and inhibition of ERK phosphorylation

MIF inhibitors have been shown to inhibit the growth of A549 non-small cell lung cancer cells, in which MIF plays an essential role for anchorage-independent growth and invasive behavior [44,45]. The growth inhibitory potency of **2d** against A549 cells was measured by a colony formation assays. A549 cells were seeded in 6-well plates with 200 cells per well. The cells were incubated for 10 days in medium containing various concentrations of the respective inhibitor. **ISO-1** was applied as a positive control. The results are shown in Fig. 7A. Inhibitor **ISO-1** inhibits colony formation at 20 and 100 μM Also treatment of A549 cell with inhibitor **2d** at 2.5, 10 and 20 μM decreased the number of colonies in a concentration−dependent manner. This demonstrates that compound **2d** inhibits cell proliferation in the clonogenic assay at 10-fold lower concentrations compared to MIF inhibitor **ISO-1**.

To gain more insight into the effect of MIF inhibitors to tumor cell proliferation, phosphorylation of ERK is investigated in A549 cells. Towards this aim the cells are incubated with **2d** or **ISO-1** before treatment with MIF. Both **2d**, as well as **ISO-1**, attenuate MIF induced ERK phosphorylation in A549 cell (Fig. 7B). Thus inhibitor **2d** is able to inhibit ERK phosphorylation and cell

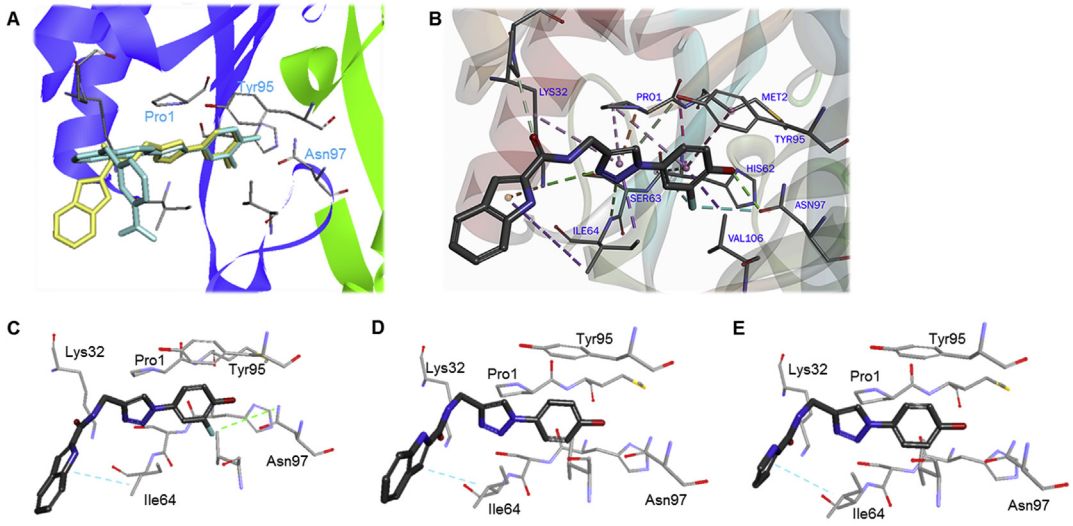

Fig. 6. Interactions between inhibitors and MIF. A) Binding of **1d** (yellow) and Jorgensen-**3bb** (cyan) to the MIF active site. The protein is shown in cartoon. Inhibitors and the residues involved in binding are displayed as sticks. B) Binding mode of compound **1d**. Compound **1d** is shown as sticks. Some residues are removed for clarity. Key residues are highlighted. C) Binding modes of compound **1d**. D) Binding modes of compound **7c.** E) Binding modes of compound **3c**. Inhibitors are shown as thick sticks and residues involved are represented by thin sticks with carbon in gray, oxygen in red and nitrogen in blue. Key interaction differences are highlighted. (For interpretation of the references to colour in this figure legend, the reader is referred to the Web version of this article.)

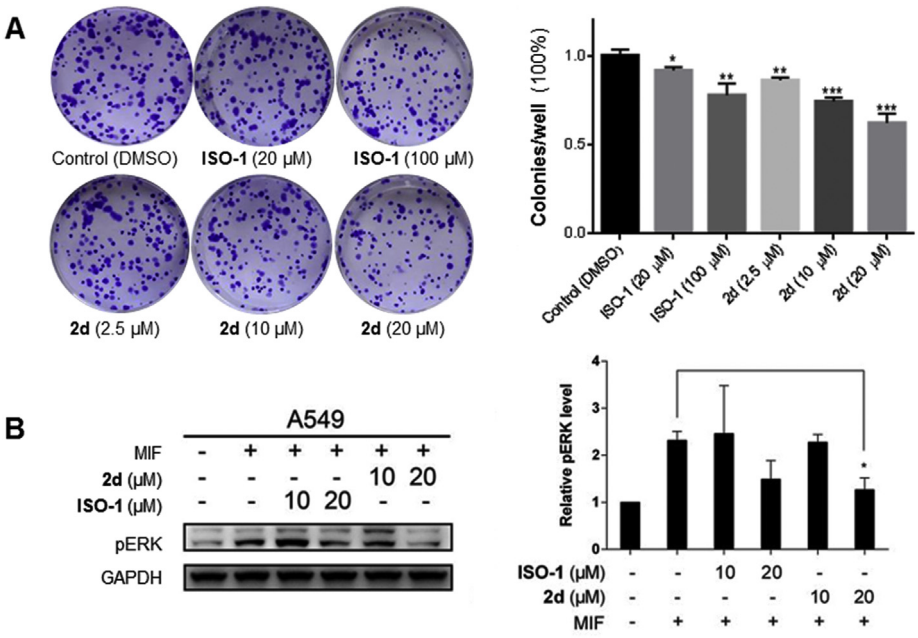

Fig. 7. MIF inhibition in A549 cells. A) A549 cells were treated with varying concentration of **ISO-1** or **2d** and stained with crystal violet. Bar chart showing the decreased number of colonies after incubation with **ISO-1** or **2d**. Colonies were counted by by ImageG and confirmed by manually counting. One colony was defined to be an aggregate of >50 cells. Data was shown as mean ± SD of three independent experiments. *p < 0.05, **p < 0.01 and ***p < 0.001 *vs* control group. B) Effect of MIF inhibitors on activated ERK signaling pathway. The cells were treated with the respective MIF inhibitors for 10 min, followed by the stimulation of 50 ng/μl MIF for 15 min at 37 °C. pERK:GAPDH ratio was applied to quantify pERK level (n = 1, duplicates will be provided). (For interpretation of the references to colour in this figure legend, the reader is referred to the Web version of this article.)

proliferation in A549 cells.

3. Conclusion

In this study, we investigated the structure-activity relationships for inhibition of MIF tautomerase activity by inhibitors with a 4-(1,2,3-triazole)-phenol core. During our studies we discovered that the transition metals copper(II) and zinc(II) inhibit MIF tautomerase activity with potencies in the low micromolar range. Addition of 0.5 mM EDTA to the assay buffer proved to be effective to avoid potential interferences from residual metal ions in inhibitor preparates. We aimed to replace the previously employed quinolone functionality by screening of a focused compound collection of 4-(1,2,3-triazole)-phenols. Several novel inhibitors were identified from which **7c** with an indole 2-carboxamide functionality proved to be the most potent one. Further improvement of potency was achieved by *ortho*-fluorination of the phenol functionality to provide **1d**. Compound **1d** proved to be a reversible and competitive inhibitor of MIF tautomerase activity with a K_i value of 3.2 μM. Binding was confirmed using an MST assay, which provided a K_D of 3.6 μM. In addition, we demonstrated that addition of a chlorine in the indole 5-position of **1d** provided compounds **2d** with further enhanced potency. This compound proved also effective in the inhibition of colony formation and attenuation of ERK signaling in A549 cells. Altogether, we present novel insights in the MIF tautomerase activity assay and we provide a novel triazole-phenol inhibitor **2d** with cellular activity, which provides a basis for further development of MIF inhibitors.

4. Experimental section

4.1. Chemistry

4.1.1. General

All the reagents and solvents were purchased from Sigma-Aldrich, AK Scientific, Fluorochem or Acros and were used without further purification. Reactions were monitored by thin layer chromatography (TLC). Merck silica gel 60 F_{254} plates were used and spots were detected with UV light. MP Ecochrom silica 32−63, 60 Å was used for column chromatography. Nuclear magnetic resonance spectra, ^{1}H NMR (500 MHz) and ^{13}C NMR (126 MHz), were recorded on a Bruker Avance 500 spectrometers. Chemical shifts were reported in ppm relative to the solvent. High-resolution mass spectra were recorded using Fourier Transform Mass Spectrometry (FTMS) and electrospray ionization (ESI) on an Applied Biosystems/SCIEX API3000-triple quadrupole mass spectrometer. Melting points were measured by Electrothermal IA9100 Melting Point Apparatus.

4.1.2. Azidophenol synthesis

Concentrated HCl (3.5 mL) was added dropwise to a solution of 4-aminophenol (1.5 g, 13.7 mmol) in water (20 mL) over a period of 5 min. After cooling the resulting solution to 0 °C, $NaNO_2$ (1.9 g, 27.5 mmol) was added portion-wise. The mixture was left stirring for 1 h at room temperature. A freshly made solution of NaN_3 (1.8 g, 27.5 mmol) in a few mL of demi-water was added dropwise to the reaction mixture and left stirring for 1h at room temperature. The reaction mixture was extracted with ethyl acetate (3x50 mL). The combined organic layers were extracted with brine and dried with $MgSO_4$, filtered and concentrated under reduced pressure. The product was obtained as a dark liquid and used without further purification.

4-azido-2-fluorophenol was prepared analogously to 4-azidophenol using 4-amino-2-fluorophenol as starting material. The product was obtained as a dark liquid and used without further purification.

4.1.3. Synthetic procedure of compounds in group A

Compounds of group A were synthesized by coupling of propiolic acid to the corresponding amines followed by CuAAC

coupling to azidophenol. Towards this aim, propiolic acid (1 eq.) and *N*,*N*′-dicyclohexylcarbodiimide (DCC, 1.0 eq.) were dissolved in dry acetonitrile (MeCN) and cooled in an ice bath for 15 min. The corresponding amines were added into the respective mixture and stirred at room temperature for 2h. The resulting precipitate was removed by filtration. The solvent was removed under reduced pressure and the products were directly used for the next step. 4-azidophenol (1.0 eq) and the appropriate alkyne (1.0 eq) were dissolved in MeOH (4 mL) in a round bottom flask equipped with stirring bar. Fresh prepared solutions of $CuSO_4$ (0.1 eq) in demi-water (0.20 mL) and sodium ascorbate (0.20 eq) in demi-water (0.20 mL) were added sequentially to the reaction mixture. The reaction mixture was left stirring overnight at 60 °C. The reaction mixture was diluted with AcOEt and then filtered. The residue was washed with a small amount of methanol. The filtrate was extracted with brine and then concentrated under reduced pressure. The residue was purified using column chromatography with CH_2Cl_2: MeOH 10:1 to yield the desired products.

*4.1.3.1. N-(3,4-dimethoxyphenyl)-1-(4-hydroxyphenyl)-1H-1,2,3-triazole-4-carboxamide (**1a**, MZ038).* Yield 77%. m.p. 250.4–253.0 °C. ^{1}H NMR (500 MHz, DMSO-d_6) δ 10.36 (s, 1H), 10.03 (s, 1H), 9.20 (s, 1H), 7.76 (d, J = 8.9 Hz, 2H), 7.54 (d, J = 2.4 Hz, 1H), 7.45 (dd, J = 8.7, 2.4 Hz, 1H), 6.96 (d, J = 8.9 Hz, 2H), 6.93 (d, J = 8.8 Hz, 1H), 3.75 (s, 3H), 3.74 (s, 3H). ^{13}C NMR (126 MHz, DMSO) δ 158.19, 157.84, 148.44, 145.26, 143.63, 132.05, 128.34, 125.01, 122.42, 116.09, 112.34, 111.84, 105.61, 55.74, 55.43. HRMS, calculated for $C_{17}H_{17}O_4N_4$ $[M+H]^+$: 341.1244, found 341.1247.

*4.1.3.2. N-(4-fluorophenyl)-1-(4-hydroxyphenyl)-1H-1,2,3-triazole-4-carboxamide (**2a**, MZ044).* Yield 30%. m.p. 252.5–254.0 °C. ^{1}H NMR (500 MHz, DMSO-d_6) δ 10.65 (s, 1H), 10.05 (s, 1H), 9.26 (s, 1H), 7.89 (dd, J = 9.1, 5.1 Hz, 2H), 7.78 (d, J = 8.9 Hz, 2H), 7.21 (t, J = 8.9 Hz, 2H), 6.97 (d, J = 8.9 Hz, 2H). ^{13}C NMR (126 MHz, DMSO) δ 158.66, 158.86 (d, J = 240.3 Hz), 143.82, 135.38 (d, J = 2.5 Hz), 128.77, 125.77, 122.85, 122.73, 122.80, 116.54, 115.68 (d, J = 22.2 Hz). ^{19}F NMR (376 MHz, DMSO-d_6) δ −118.70 (tt, J = 9.3, 5.1 Hz). HRMS, calculated for $C_{15}H_{12}O_2N_4F$ $[M+H]^+$: 299.0939, found 299.0939.

*4.1.3.3. N-(2-fluorophenyl)-1-(4-hydroxyphenyl)-1H-1,2,3-triazole-4-carboxamide (**3a**, ZP034).* Yield 53%. m.p. 224.8–226.3 °C. ^{1}H NMR (500 MHz, DMSO-d_6) δ 10.16 (s, 1H), 10.05 (s, 1H), 9.28 (s, 1H), 7.77 (d, J = 8.8 Hz, 2H), 7.74 (d, J = 5.4 Hz, 1H), 7.36–7.20 (m, 3H), 6.96 (d, J = 8.7 Hz, 2H). ^{13}C NMR (126 MHz, DMSO) δ 158.65, 156.64, 154.68, 143.24, 128.77, 127.17, 126.53, 125.77, 125.61, 124.88, 122.87, 116.55, 116.22. ^{19}F NMR (376 MHz, DMSO-d_6) δ −122.20 (ddd, J = 9.3, 7.1, 4.2 Hz). HRMS, calculated for $C_{15}H_{12}O_2N_4F$ $[M+H]^+$: 299.0939, found 299.0936.

*4.1.3.4. N-(2-aminophenyl)-1-(4-hydroxyphenyl)-1H-1,2,3-triazole-4-carboxamide (**4a**, ZP039).* Yield 86%. Decomposed at 250 °C. ^{1}H NMR (500 MHz, DMSO-d_6) δ 10.04 (s, 1H), 9.82 (s, 1H), 9.22 (s, 1H), 7.76 (d, J = 8.6 Hz, 2H), 7.30 (d, J = 7.6 Hz, 1H), 6.97 (m,3H), 6.80 (d, J = 7.8 Hz, 1H), 6.62 (t, J = 7.4 Hz, 1H), 4.93 (s, 2H). ^{13}C NMR (126 MHz, DMSO) δ 158.67, 143.89, 143.08, 128.85, 126.86, 126.53, 125.44, 123.50, 122.87, 122.72, 117.10, 116.94, 116.57. HRMS, calculated for $C_{15}H_{14}O_2N_5$ $[M+H]^+$: 296.1142, found 296.1140.

*4.1.3.5. 1-(4-hydroxyphenyl)-N-phenyl-1H-1,2,3-triazole-4-carboxamide (**5a**, ZP042).* Yield 54%. m.p. 232.2–232.6 °C. ^{1}H NMR (500 MHz, DMSO-d_6) δ 10.53 (s, 1H), 10.06 (s, 1H), 9.26 (s, 1H), 7.87 (d, J = 8.2 Hz, 2H), 7.78 (d, J = 8.4 Hz, 2H), 7.37 (t, J = 7.8 Hz, 2H), 7.12 (t, J = 7.3 Hz, 1H), 6.97 (d, J = 8.4 Hz, 2H). ^{13}C NMR (126 MHz, DMSO) δ 158.23, 158.21, 143.48, 138.52, 128.63, 128.32, 125.26, 123.84, 122.38, 120.45, 116.08. HRMS, calculated for $C_{15}H_{13}O_2N_4$ $[M+H]^+$: 281.1033, found 281.1031.

*4.1.3.6. N-cyclopropyl-1-(4-hydroxyphenyl)-1H-1,2,3-triazole-4-carboxamide (**6a**, MZ049).* Yield 42%. m.p. 233.2–233.5 °C. ^{1}H NMR (500 MHz, DMSO-d_6) δ 10.02 (s, 1H), 9.07 (s, 1H), 8.65 (d, J = 4.3 Hz, 1H), 7.73 (d, J = 8.6 Hz, 2H), 6.94 (d, J = 8.6 Hz, 2H), 2.88 (dt, J = 10.1, 4.9 Hz, 1H), 0.72–0.63 (m, 4H). ^{13}C NMR (126 MHz, DMSO) δ 161.18, 158.54, 143.90, 128.84, 124.68, 122.73, 116.51, 23.01, 6.18. HRMS, calculated for $C_{12}H_{13}O_2N_4$ $[M+H]^+$: 245.1033, found 245.1031.

*4.1.3.7. Ethyl (1-(4-hydroxyphenyl)-1H-1,2,3-triazole-4-carbonyl) glycinate (**7a**, MZ053).* Yield 78%. Decomposed at 220 °C. ^{1}H NMR (500 MHz, DMSO-d_6) δ 10.04 (s, 1H), 9.14 (s, 1H), 8.95 (t, J = 6.0 Hz, 1H), 7.75 (d, J = 8.8 Hz, 2H), 6.95 (d, J = 8.9 Hz, 2H), 4.13 (q, J = 7.1 Hz, 2H), 4.02 (d, J = 6.1 Hz, 2H), 1.22 (t, J = 7.1 Hz, 3H). ^{13}C NMR (126 MHz, DMSO-d_6) δ 170.09, 160.42, 158.62, 143.32, 128.80, 125.11, 122.74, 116.51, 60.99, 41.19, 14.54. HRMS, calculated for $C_{13}H_{15}O_4N_4$ $[M+H]^+$: 291.1088, found 291.1086.

4.1.4. Synthetic procedure of compounds in group B

For compounds of group B, 0.5 mmol of 4-azidophenol (1.0 eq) and the 0.5 mmol appropriate alkyne (1.0 eq) were dissolved in MeOH (4 mL) in a round bottom flask. Fresh prepared solutions of $CuSO_4$ (0.1 eq) in demi-water (0.20 mL) and sodium ascorbate (0.20 eq) in demi-water (0.20 mL) were added sequentially to the reaction mixture. The reaction mixture was left stirring overnight at room temperature. The reaction mixture was diluted with AcOEt and precipitate was removed by filtration. The residue was washed with methanol. The filtrate was extracted with brine and then concentrated under reduced pressure. The residue was purified using column chromatography with CH_2Cl_2: MeOH 50:1 to yield the desired products.

*4.1.4.1. 4-(4-(hydroxymethyl)-1H-1,2,3-triazol-1-yl)phenol (**1b**, MZ028).* Yield 21%. m.p. 212.5–213.8 °C. ^{1}H NMR (500 MHz, DMSO-d_6) δ 9.92 (s, 1H), 8.49 (s, 1H), 7.66 (d, J = 8.9 Hz, 2H), 6.93 (d, J = 8.9 Hz, 2H), 5.29 (t, J = 5.6 Hz, 1H), 4.59 (d, J = 5.5 Hz, 2H). ^{13}C NMR (126 MHz, DMSO) δ 158.04, 149.19, 129.41, 122.26, 121.34, 116.47, 55.44. HRMS, calculated for $C_9H_{10}O_2N_3$ $[M+H]^+$: 192.0768, found 192.0769.

*4.1.4.2. 4-(4-(1-hydroxyethyl)-1H-1,2,3-triazol-1-yl)phenol (**2b**, MZ043).* Yield 96%. m.p. 89.9–90.3 °C. ^{1}H NMR (500 MHz, DMSO-d_6) δ 9.91 (s, 1H), 8.44 (s, 1H), 7.66 (d, J = 8.5 Hz, 2H), 6.92 (d, J = 8.5 Hz, 2H), 5.34 (d, J = 4.0 Hz, 1H), 4.93–4.85 (m, 1H), 1.47 (d, J = 6.3 Hz, 3H). ^{13}C NMR (126 MHz, DMSO-d_6) δ 157.99, 129.47, 119.94, 116.45, 62.02. HRMS, calculated for $C_{10}H_{12}O_2N_3$ $[M+H]^+$: 206.0924, found 206.0925.

*4.1.4.3. 4-(4-Isopropyl-1H-1,2,3-triazol-1-yl)phenol (**3b**, ZP180).* Yield 52%. ^{1}H NMR (500 MHz, Methanol-d_4) δ 8.15 (s, 1H), 7.62 (d, J = 8.9 Hz, 2H), 6.96 (d, J = 8.9 Hz, 2H), 3.14 (m, 1H), 1.38 (d, J = 7.0 Hz, 6H). ^{13}C NMR (126 MHz, Methanol-d_4) δ 158.03, 154.60, 129.51, 121.90, 118.74, 115.70, 25.66, 21.49. HRMS, calculated for $C_{11}H_{13}ON_3$ $[M+H]^+$: 204.1131, found 204.1131.

*4.1.4.4. 4-(4-Propyl-1H-1,2,3-triazol-1-yl)phenol (**4b**, MZ018).* Yield 12%. ^{1}H NMR (500 MHz, Chloroform-*d*) δ 9.89 (s, 1H), 8.37 (s, 1H), 7.63 (d, J = 8.9 Hz, 2H), 6.91 (d, J = 8.9 Hz, 2H), 2.64 (t, J = 7.5 Hz, 2H), 1.66 (m, 2H), 0.94 (t, J = 7.4 Hz, 3H). ^{13}C NMR (126 MHz, DMSO) δ 157.45, 147.58, 129.05, 121.63, 120.03, 115.98, 27.10, 22.19, 13.67. HRMS, calculated for $C_{11}H_{14}ON_3$ $[M+H]^+$: 204.1131, found 204.1129.

*4.1.4.5. 4-(4-Pentyl-1H-1,2,3-triazol-1-yl)phenol (**5b**, ZP085).* Yield 67%. m.p. 93.2–94.0 °C. ^{1}H NMR (500 MHz, DMSO-d_6) δ 9.88 (s, 1H), 8.38 (s, 1H), 7.64 (d, J = 8.8 Hz, 2H), 6.92 (d, J = 8.8 Hz, 2H), 2.67 (t, J = 7.6 Hz, 2H), 1.66 (m, 2H), 1.33 (m, 4H), 0.89 (t, J = 7.4 Hz, 3H). ^{13}C NMR (126 MHz, DMSO) δ 157.90, 148.24, 129.51, 122.01, 120.42, 116.42, 31.31, 29.05, 25.46, 22.36, 14.38. HRMS, calculated for $C_{13}H_{18}ON_3$ $[M+H]^+$: 232.1444, found 232.1442.

*4.1.4.6. 4-(4-Cyclohexyl-1H-1,2,3-triazol-1-yl)phenol (**6b**, ZP179).* Yield 46%. ^{1}H NMR (500 MHz, DMSO-d_6) δ 9.89 (s, 1H), 8.36 (s, 1H), 7.64 (d, J = 8.8 Hz, 2H), 6.92 (d, J = 8.8 Hz, 2H), 2.72 (t, J = 10.9 Hz, 1H), 2.01 (d, J = 11.3 Hz, 2H), 1.77 (d, J = 12.0 Hz, 2H), 1.69 (d, J = 12.7 Hz, 1H), 1.41 (m, 4H), 1.24 (m, 1H). ^{13}C NMR (126 MHz, DMSO) δ 157.88, 153.42, 129.57, 122.12, 119.29, 116.42, 35.13, 33.03, 25.95. HRMS, calculated for $C_{14}H_{17}ON_3$ $[M+H]^+$: 244.1444, found 244.1443.

*4.1.4.7. 4-(4-(hex-5-yn-1-yl)-1H-1,2,3-triazol-1-yl)phenol (**7b**, MZ014).* Yield 21%. Decomposed at 220 °C. ^{1}H NMR (500 MHz, DMSO-d_6) δ 9.88 (s, 1H), 8.38 (s, 1H), 7.63 (d, J = 8.9 Hz, 2H), 6.91 (d, J = 8.9 Hz, 2H), 2.77 (t, J = 2.6 Hz, 1H), 2.69 (t, J = 7.6 Hz, 2H), 2.21 (td, J = 7.1, 2.6 Hz, 2H), 1.73 (m, 2H), 1.52 (m, 2H). ^{13}C NMR (126 MHz, DMSO) δ 157.92, 147.92, 129.49, 122.12, 120.48, 116.44, 84.87, 71.80, 28.41, 27.93, 24.93, 17.91. HRMS, calculated for $C_{14}H_{16}ON_3$ $[M+H]^+$: 242.1288, found 242.1298.

*4.1.4.8. 4-(4-Octyl-1H-1,2,3-triazol-1-yl)phenol (**8b**, ZP087).* Yield 30%. m.p. 103.8–105.2 °C. ^{1}H NMR (500 MHz, DMSO-d_6) δ 9.91 (s, 1H), 8.37 (s, 1H), 7.63 (d, J = 8.4 Hz, 2H), 6.92 (d, J = 8.5 Hz, 2H), 2.66 (t, J = 7.6 Hz, 2H), 1.64 (m, 2H), 1.35–1.22 (m, 10H), 0.86 (t, J = 6.7 Hz, 3H). ^{13}C NMR (126 MHz, DMSO) δ 157.89, 148.27, 129.51, 122.04, 120.39, 116.43, 31.76, 29.35, 29.24, 29.10, 25.49, 25.46, 22.57, 14.43. HRMS, calculated for $C_{16}H_{24}ON_3$ $[M+H]^+$: 274.1914, found 274.1911.

*4.1.4.9. Methyl 4-(1-(4-hydroxyphenyl)-1H-1,2,3-triazol-4-yl)butanoate (**9b**, MZ056).* Yield 17%. m.p. 89.9–90.3 °C. ^{1}H NMR (500 MHz, DMSO-d_6) δ 9.90 (s, 1H), 8.40 (s, 1H), 7.63 (d, J = 8.8 Hz, 2H), 6.91 (d, J = 8.9 Hz, 2H), 3.59 (s, 3H), 2.70 (t, J = 7.6 Hz, 2H), 2.40 (t, J = 7.4 Hz, 2H), 1.91 (m, 2H). ^{13}C NMR (126 MHz, DMSO) δ 173.75, 157.91, 129.42, 122.20, 120.78, 116.48, 51.76, 33.08, 24.69, 24.58. HRMS, calculated for $C_{13}H_{16}O_3N_3$ $[M+H]^+$: 262.1186, found 262.1184.

*4.1.4.10. 3-(1-(4-hydroxyphenyl)-1H-1,2,3-triazol-4-yl)-N-phenylpropanamide (**10b**, ZP078).* Yield 27%. m.p. 190.9–192.0 °C. ^{1}H NMR (500 MHz, DMSO-d_6) δ 9.99 (s, 1H), 9.90 (s, 1H), 8.38 (s, 1H), 7.60 (m, 4H), 7.28 (t, J = 7.9 Hz, 2H), 7.02 (t, J = 7.4 Hz, 1H), 6.91 (d, J = 8.9 Hz, 2H), 3.01 (t, J = 7.5 Hz, 2H), 2.75 (t, J = 7.6 Hz, 2H). ^{13}C NMR (126 MHz, DMSO) δ 170.62, 157.99, 147.18, 139.67, 129.41, 129.14, 123.52, 122.16, 120.68, 119.52, 116.48, 36.09, 21.47. HRMS, calculated for $C_{17}H_{17}O_2N_4$ $[M+H]^+$: 309.1346, found 309.1343.

4.1.5. Synthetic procedure of compounds in group C

For compounds of group C, 0.5 mmol 2-propynylamine was used to form amides with corresponding carboxylic acid derivatives mediated by *N,N′*-dicyclohexylcarbodiimide (DCC, 1.0 eq.) in dry acetonitrile (MeCN). Conditions and procedures used here were same as these in group A. Afterwards, different amides were mixed with 4-azidophenol (1.0 eq), fresh prepared solutions of $CuSO_4$ (0.1 eq) in demi-water (0.20 mL), sodium ascorbate (0.20 eq) in demi-water (0.20 mL) in MeOH (4 mL). The reaction mixture was left stirring overnight for at 60 °C. The CuAAC reaction and purification were also done in the same way as for group A described above.

*4.1.5.1. N-((1-(4-hydroxyphenyl)-1H-1,2,3-triazol-4-yl)methyl)benzamide (**1c**, ZP049).* Yield 28%. m.p. 229.1–230.6 °C. ^{1}H NMR (500 MHz, DMSO-d_6) δ 9.90 (s, 1H), 9.04 (t, J = 5.2 Hz, 1H), 8.48 (s, 1H), 7.90 (d, J = 7.5 Hz, 2H), 7.66 (d, J = 8.5 Hz, 2H), 7.52 (t, J = 7.1 Hz, 1H), 7.46 (m, 2H), 6.91 (d, J = 8.5 Hz, 2H), 4.59 (d, J = 4.8 Hz, 2H). ^{13}C NMR (126 MHz, DMSO) δ 166.22, 157.64, 134.14, 131.34, 131.29, 128.88, 128.28, 127.36, 121.80, 121.16, 116.02, 34.89. HRMS, calculated for $C_{16}H_{15}O_2N_4$ $[M+H]^+$: 295.1189, found 295.1189.

*4.1.5.2. N-((1-(4-hydroxyphenyl)-1H-1,2,3-triazol-4-yl)methyl)thiophene-2-carboxamide (**2c**, ZP054).* Yield 40%. m.p. 235.2–237.1 °C. ^{1}H NMR (500 MHz, DMSO-d_6) δ 9.91 (s, 1H), 9.07 (bs, 1H), 8.49 (s, 1H), 7.80 (d, J = 2.4 Hz, 1H), 7.76 (d, J = 3.9 Hz, 1H), 7.66 (d, J = 7.9 Hz, 2H), 7.19–7.11 (m, 1H), 6.91 (d, J = 7.8 Hz, 2H), 4.55 (d, J = 3.5 Hz, 2H). ^{13}C NMR (126 MHz, DMSO) δ 161.16, 157.67, 139.70, 130.95, 128.87, 128.44, 128.29, 127.97, 121.86, 121.30, 116.05, 34.66. HRMS, calculated for $C_{14}H_{13}O_2N_4S$ $[M+H]^+$: 301.0754, found 301.0753.

*4.1.5.3. N-((1-(4-hydroxyphenyl)-1H-1,2,3-triazol-4-yl)methyl)-1H-pyrrole-2-carboxamide (**3c**, ZP063).* Yield 15%. m.p. 244.1–246.2 °C. ^{1}H NMR (500 MHz, DMSO-d_6) δ 11.44 (s, 1H), 9.92 (s, 1H), 8.52 (s, 1H), 8.44 (s, 1H), 7.65 (d, J = 8.7 Hz, 2H), 6.91 (d, J = 8.7 Hz, 2H), 6.86 (d, J = 2.7 Hz, 1H), 6.81 (d, J = 3.8 Hz, 1H), 6.07 (m, 1H), 4.53 (d, J = 3.5 Hz, 2H). ^{13}C NMR (126 MHz, DMSO) δ 160.59, 157.63, 146.10, 128.88, 126.03, 121.83, 121.45, 121.01, 116.02, 110.29, 108.60, 34.09. HRMS, calculated for $C_{14}H_{14}O_2N_5$ $[M+H]^+$: 284.1142, found 284.1140.

*4.1.5.4. 5-Bromo-N-((1-(4-hydroxyphenyl)-1H-1,2,3-triazol-4-yl)methyl)furan-2-carboxamide (**4c**, ZP064).* Yield 22%. m.p. 204.7–205.0 °C. ^{1}H NMR (500 MHz, DMSO-d_6) δ 9.93 (s, 1H), 9.02 (bs, 1H), 8.47 (s, 1H), 7.65 (d, J = 8.1 Hz, 2H), 7.19 (d, J = 3.6 Hz, 1H), 6.91 (d, J = 8.0 Hz, 2H), 6.77 (d, J = 3.9 Hz, 1H), 4.53 (d, J = 4.5 Hz, 2H). ^{13}C NMR (126 MHz, DMSO) δ 158.10, 157.14, 150.01, 145.90, 129.30, 124.98, 122.27, 121.60, 121.53, 116.48, 114.42, 34.62. HRMS, calculated for $C_{14}H_{12}O_3N_4Br$ $[M+H]^+$: 363.0087, found 363.0086.

*4.1.5.5. N-((1-(4-hydroxyphenyl)-1H-1,2,3-triazol-4-yl)methyl)-5-methylthiophene-2-carboxamide (**5c**, ZP065).* Yield 38%. m.p. 225.9–227.7 °C. ^{1}H NMR (500 MHz, DMSO-d_6) δ 9.93 (s, 1H), 8.95 (s, 1H), 8.49 (s, 1H), 7.66 (d, J = 8.4 Hz, 2H), 7.60 (d, J = 3.0 Hz, 1H), 6.91 (d, J = 8.4 Hz, 2H), 6.83 (d, J = 3.3H, 1H), 4.53 (d, J = 4.5 Hz, 2H), 2.45 (s, 3H). ^{13}C NMR (126 MHz, DMSO) δ 161.09, 157.63, 145.83, 144.70, 137.11, 128.84, 128.50, 126.39, 121.79, 121.23, 116.00, 34.55, 15.20. HRMS, calculated for $C_{15}H_{15}O_2N_4S$ $[M+H]^+$: 315.0910, found 315.0907.

*4.1.5.6. 4-Fluoro-N-((1-(4-hydroxyphenyl)-1H-1,2,3-triazol-4-yl)methyl)benzamide (**6c**, ZP069).* Yield 31%. m.p. 248.0–249.4 °C. ^{1}H NMR (500 MHz, DMSO-d_6) δ 9.92 (s, 1H), 9.08 (t, J = 5.6 Hz, 1H), 8.49 (s, 1H), 7.97 (dd, J = 8.7, 5.6 Hz, 2H), 7.65 (d, J = 8.9 Hz, 2H), 7.30 (t, J = 8.8 Hz, 2H), 6.91 (d, J = 8.9 Hz, 2H), 4.58 (d, J = 5.6 Hz, 2H). ^{13}C NMR (126 MHz, DMSO) δ 165.16, 163.94 (d, J = 248.4 Hz), 157.62, 145.77, 130.64 (d, J = 2.9 Hz), 130.03 (d, J = 14.2 Hz), 130.08, 129.97, 128.87, 121.81, 121.08, 115.98, 115.21 (d, J = 21.8 Hz) 39.85, 39.69, 34.92. ^{19}F NMR (376 MHz, DMSO-d_6) δ −119.43 (tt, J = 9.0, 5.1 Hz). HRMS, calculated for $C_{16}H_{14}O_2N_4F$ $[M+H]^+$: 313.1095, found 313.1093.

*4.1.5.7. N-((1-(4-hydroxyphenyl)-1H-1,2,3-triazol-4-yl)methyl)-1H-indole-2-carboxamide (**7c**, ZP071).* Yield 22%. m.p. 246.8–250.0 °C. ^{1}H NMR (500 MHz, DMSO-d_6) δ 11.59 (s, 1H), 9.92 (s, 1H), 9.04 (t, J = 5.7 Hz, 1H), 8.50 (s, 1H), 7.66 (d, J = 8.9 Hz, 2H), 7.61 (d, J = 8.0 Hz, 1H), 7.43 (d, J = 8.2 Hz, 1H), 7.20–7.15 (m, 2H), 7.03 (t, J = 7.5 Hz, 1H), 6.91 (d, J = 8.9 Hz, 2H), 4.62 (d, J = 5.6 Hz, 2H). ^{13}C NMR (126 MHz,

DMSO) δ 161.09, 157.66, 145.73, 136.47, 131.49, 128.87, 127.09, 123.35, 121.85, 121.54, 121.13, 119.73, 116.03, 112.33, 102.86, 34.41. HRMS, calculated for $C_{18}H_{16}O_2N_5$ $[M+H]^+$: 334.1299, found 334.1297.

*4.1.5.8. N-((1-(4-hydroxyphenyl)-1H-1,2,3-triazol-4-yl)methyl)-2-(1H-indol-2-yl)acetamide (**8c**, ZP075).* Yield 47%. m.p. 225.9–226.8 °C. ^{1}H NMR (500 MHz, DMSO-d_6) δ 10.88 (s, 1H), 9.93 (s, 1H), 8.46 (t, J = 5.6 Hz, 1H), 8.23 (s, 1H), 7.55 (m, 3H), 7.34 (d, J = 8.1 Hz, 1H), 7.21 (d, J = 2.2 Hz, 1H), 7.06 (s, 1H), 6.96 (d, J = 7.6 Hz, 1H), 6.91 (d, J = 8.9 Hz, 2H), 4.36 (d, J = 5.6 Hz, 2H), 3.56 (s, 2H). ^{13}C NMR (126 MHz, DMSO) δ 170.87, 157.67, 145.88, 136.14, 128.80, 127.22, 123.94, 121.76, 120.98, 120.80, 118.77, 118.35, 116.07, 111.38, 108.80, 34.40, 32.66. HRMS, calculated for $C_{19}H_{18}O_2N_5$ $[M+H]^+$: 348.1455, found 348.1453.

4.1.6. Synthetic procedure of compounds in group D

2-fluoro-4-nitrophenol (1.15 g, 7.3 mmol) was dissolved in ethanol (10 mL) and added to Pd/C (66 mg). Subsequently the flask was charged with hydrogen (H_2) gas and the black suspension was stirred at room temperature for 4 h. After 4 h the starting material disappeared as analyzed by TLC. The resulting mixture was filtered and the solvent was evaporated under reduced pressure to provide the crude product that was used directly for the next reaction step. The crude product was dissolve in water (10 mL) with concentrated HCl (2 mL). Subsequently, $NaNO_2$ (1.0 g, 15 mmol) and NaN_3 (0.95 g, 15 mmol) were added sequentially to yield 4-azido-2-fluorophenol. ^{1}H NMR (500 MHz, DMSO-d_6) δ 9.94 (s, 1H), 7.06–6.90 (m, 2H), 6.79 (d, J = 6.3 Hz, 1H). ^{13}C NMR (126 MHz, DMSO-d_6) δ 151.67 (d, J = 242.8 Hz), 142.89 (d, J = 12.1 Hz), 130.75 (d, J = 8.6 Hz), 119.09, 115.70, 108.26 (d, J = 22.0 Hz).

Subsequently, 0.25 mmol of the required alkynes was synthesized as described above by dissolving 2-propynylamine (0.25 mmol) with the corresponding carboxylic acids (0.25 mmol) in dry acetonitrile (MeCN). Subsequently, *N,N′*-dicyclohexylcarbodiimide (DCC, 1.0 eq.) was added as a coupling reagent. The reactants mixtures were stirred at 60 °C for overnight. The products were purified following the same methods as methods used to purify compounds in group C.

*4.1.6.1. N-((1-(3-fluoro-4-hydroxyphenyl)-1H-1,2,3-triazol-4-yl)methyl)-1H-indole-2-carboxamide (**1d**, ZP086).* Yield 41%. m.p. 253.6–254.3 °C. ^{1}H NMR (500 MHz, DMSO-d_6) δ 11.59 (s, 1H), 10.38 (s, 1H), 9.05 (t, J = 5.7 Hz, 1H), 8.59 (s, 1H), 7.77 (dd, J = 11.9, 2.5 Hz, 1H), 7.60 (d, J = 8.0 Hz, 1H), 7.56 (d, J = 8.8 Hz, 1H), 7.43 (d, J = 8.2 Hz, 1H), 7.19–7.15 (m, 2H), 7.10 (t, J = 9.0 Hz, 1H), 7.03 (t, J = 7.5 Hz, 1H), 4.62 (d, J = 5.6 Hz, 2H). ^{13}C NMR (126 MHz, DMSO) δ 161.56, 151.18 (d, J = 242.7 Hz), 146.45, 145.68 (d, J = 11.9 Hz), 136.92, 131.90, δ 128.99 (d, J = 8.7 Hz), 127.53, 123.82, 122.00 (d, J = 19.1 Hz), 121.67 (d, J = 6.1 Hz), 120.20, 118.69, 117.04 (d, J = 16.3 Hz), 112.77, 109.50, 103.32, 34.82. ^{19}F NMR (376 MHz, DMSO-d_6) δ −133.75 to −133.81 (m). HRMS, calculated for $C_{18}H_{15}O_2N_5F$ $[M+H]^+$: 352.1204, found 352.1205.

*4.1.6.2. 5-Chloro-N-((1-(3-fluoro-4-hydroxyphenyl)-1H-1,2,3-triazol-4-yl)methyl)-1H-indole-2-carboxamide (**2d**, ZP094).* Yield 35%. ^{1}H NMR (500 MHz, DMSO-d_6) δ 11.59 (s, 1H), 10.38 (s, 1H), 9.05 (t, J = 5.7 Hz, 1H), 8.59 (s, 1H), 7.77 (dd, J = 11.9, 2.5 Hz, 1H), 7.60 (d, J = 8.0 Hz, 1H), 7.56 (d, J = 8.8 Hz, 1H), 7.43 (d, J = 8.2 Hz, 1H), 7.19–7.15 (m, 2H), 7.10 (t, J = 9.0 Hz, 1H), 7.03 (t, J = 7.5 Hz, 1H), 4.62 (d, J = 5.6 Hz, 2H). ^{13}C NMR (126 MHz, DMSO) δ 161.18, 151.17 (d, J = 242.6 Hz), 146.31, 145.68 (d, J = 11.9 Hz), 135.31, 133.42, 128.98 (d, J = 8.9 Hz), 128.59, 124.69, 123.92, 121.68 (d, J = 4.5 Hz), 121.07 (d, J = 18.3 Hz), 118.68, 117.03(d, J = 16.3 Hz), 114.38, 109.49, 102.89, 34.86. HRMS, calculated for $C_{18}H_{14}O_2N_5ClF$ $[M+H]^+$: 386.0820, found 386.0823.

4.2. Enzyme activity study

4.2.1. Protein expression and purification

C-terminal His-tagged recombinant human MIF was expressed with pET-20b(+) plasmid and Escherichia coli BL21 according to literature procedures [46]. After culturing *Escherichia coli* cells were pelleted by centrifugation at 4000 rpm for 20 min. Cell pellets were resuspended in a lysis buffer containing 20 mM Tris- HCl (titrated to pH 7.5 with an aqueous concentrated NaOH solution), 20 mM sodium chloride, 10% glycerol, 2 mM magnesium chloride, and 0.2 × complete EDTA-free protease inhibitor cocktail (Roche). Subsequently, the cells were lysed by sonication and centrifuged at 17,000 g for 20 min. The supernatant was purified by medium pressure chromatography system (Biologic Duoflow) equipped with a His trap HP (5 mL) column with detection at 280 nm for the eluent. The binding buffer contained 50 mM Tris and 10% glycerol that was titrated to pH 7.4 using 1 M NaOH or 1 M HCl. The elution buffer contained 500 mM imidazole, 50 mM Tris, 10% glycerol that is also titrated to pH 7.4 using 1 M NaOH or 1 M HCl. The collected protein was purified again by PD-10 column (GE healthcare) to remove the high concentration of imidazole. The resulting MIF was assessed by SDS gel electrophoresis and no impurities were observed (>95%). The concentration of MIF was determined by Bradford protein assay to be 1.83 mg/mL (135 μM). The purified protein was aliquoted and stored at −80 °C. The stability of the protein was tested by the tautomerase assays (Synergy H1 Hybrid Reader, BioTek) and thermal stability assays (nanoDSF, Prometheus NT.48).

4.2.2. Tautomerase assay

Inhibition of the tautomerase activity and kinetics of MIF was measured using 4-hydroxyphenyl pyruvic acid (4-HPP) as substrate. A stock solution was prepared by dissolution of 4-HPP in 50 mM ammonium acetate buffer that was titrated to pH 6.0 using 1.0 M NaOH or 1.0 M HCl. 4-HPP was dissolved to provide a concentration of 10 mM and this solution was incubated overnight at room temperature to allow equilibration of the keto and enol forms. Subsequently this 4-HPP stock solution was stored at 4 °C. The MIF stock solution (80 μL, 135 μM MIF) was diluted in the boric acid buffer to provide a MIF solution (12 mL, 0.9 μM) in boric acid buffer (435 mM, pH 6.2). The enzyme activity was determined by premixing 170 μL of the MIF dilution with 10 μL EDTA (20 mM in demiwater) and DMSO (20 μL). This mixture was pre-incubated for 15 min. Next, 50 μL of this mixture was mixed with 50 μL of 1 mM 4-HPP solution in 50 mM pH 6.0 ammonium acetate buffer. Subsequently, MIF tautomerase activity was monitored by formation of the borate–enol complex, which was measured by the increase in UV absorbance at 305 nm.The increase in UV absorbance was monitored over the first 10 min of incubation using a BioTek Synergy H1 Hybrid plate reader. In experiments where EDTA was excluded the 10 μL of the 20 mM EDTA solution is replaced for demi water. Inhibitors were added to the experiment as DMSO solutions by replacing the blank DMSO for a DMSO solution with a corresponding inhibitors concentration that provides the final inhibitors concentration after dilution. Initially, the inhibitors were dissolved in DMSO at 10 mM, which was diluted further in DMSO to provide 1 mM from which 20 μL was added to the enzyme activity assay to provide a final concentration of 50 μM in the screening. For compounds that showed ca. 50% or greater inhibition at 50 μM, an IC_{50} was measured. Towards this aim the compounds were stepwise diluted in DMSO and subsequently the MIF tautomerase activity was measured using the same protocol. The DMSO concentration in all assays was kept constant at 5% and control experiments

demonstrated that this DMSO concentration did not influence the tautomerase activity. MIF tautomerase activity in the presence of blank DMSO was set to 100% enzyme activity. In the negative control the enzyme was excluded to monitor non-catalyzed conversion of the substrate, which did not show a change in absorbance at 305 nm. Data from the first 3 min were used to calculate the initial velocities and the nonlinear regression analyses for the enzyme kinetics were repeated three times with the program Prism6 (GraphPad).

4.3. Docking study

Docking studies were performed to gain insight in the structure-activity relationships. All molecular modelings were done with the program Discovery studio (Dassault systems) version 2018 and the crystal structures of human recombinant MIF (PDB-code:4wrb, [42], 5hvs [32]) were used. The CDOCKER protocol was used for docking which is a CHARMM based algorithm. Docking was verified by use of the ligand 3-((6-(1-(3-fluoro-4-hydroxyphenyl)-1H-1,2,3-triazol-4-yl)naphthalen-1-yl)oxy)benzoic acid (Jorgensen-**3bb**) from the crystal structure 5hvs. This ligand contains the 4-(1,2,3-triazole)phenol functionality, which is also present in our molecules. First, the ligand was removed from the protein and subsequently docked back in the crystal structure. All 10 highest ranked poses show a comparable position compared to the original pose from the crystal structure in the 4-(1,2,3-triazole)phenol functionality (Fig. S8). Poses with the lowest CDOCKER energies were chosen for representation.

4.4. MST

MST experiments were performed on a Monolith NT.115 system (NanoTemper Technologies) using 100% LED and 20% IR-laser power. Laser on and off times were set at 30s and 5s, respectively. Recombinant His-tagged MIF was labeled with RED-tris-NTA for 30 min (NanoTemper Technologies) and applied at a final concentration of 50 nM. A two-fold dilution series was prepared for compound **1d** in PBS-T with 5% DMSO. Subsequently, 10 μL of labeled MIF was mixed with 10 μL samples with different concentration of compound **1d**. Samples were filled into hydrophilic capillaries (Monolith NT.115 capillary, standard treated) for measurement.

4.5. Colony formation assay

A549 cells were seeded in 6-well plates, each well contained 2 mL medium with 200 A549 cells and incubated for 24 h. 10 mM stock solutions of **ISO-1** or **2d** were prepared by dissolution in DMSO. Subsequently, the inhibitors were diluted to different concentration in fresh medium before addition into the corresponding well upon which the cells were treated continuously for 10 days. Finally, the cells were fixed with paraformaldehyde for 20 min and stained with crystal violet for 20 min. After washing, the image of each well was photographed and analyzed with ImageG. We defined one colony as an aggregate of >50 cells. The numbers of colonies was analyzed as the ratio of the numbers found in inhibitor treated samples compared to untreated samples.

4.6. ERK signaling pathway study

Cells were seeded into a 6-well plate at a density of 2×10^5 cells per well with RPMI-1640 medium containing 10% fetal bovine serum (FBS) (Costar Europe, Badhoevedorp, The Netherlands), and 1% penicillin/streptomycin. After overnight culturing, the cells were treated with the respective MIF inhibitors for 10 min, followed by the stimulation of 50 ng/μl MIF for 15 min. After that, cells were lysed by RIPA buffer. The BCA Protein Assay Kit (Pierce, Rockford IL, USA) was used to determine the protein concentration according to the manufacturing instruction. Thirty-microgram protein was separated by a pre-cast 10% NuPAGE Bis-Tris gel (Invitrogen, USA). The separated proteins were transferred to a polyvinylidene difluoride (PVDF) membrane. Five percent skimmed milk was used to block the membrane for 1 h at RT. The blocked membrane was incubated with appropriate primary antibody (phosphor-ERK, pERK, #9101, 1:1000, Cell Signaling; GAPDH, #97166, 1:10000, Cell Signaling) overnight at 4 °C, followed by the treatment of an HRP-conjugated secondary goat anti-rabbit antibody (#P0448, 1:2000) or rabbit anti-mouse antibody (#P0260, 1:2000) (Dako Cytomation, Glostrup, Denmark) at RT for 1 h. The protein bands were visualized with enhanced chemiluminescence (ECL) solution (GE Healthcare, Amersham, UK). The figures were quantified with imageJ software (National Institutes of Health, USA) based on greyscale.

Declaration of competing interest

The authors declare that they have no known competing financial interests or personal relationships that could have appeared to influence the work reported in this paper.

Acknowledgements

Z. X. acknowledges funding from the China Scholarship Council (File No. 201706010341). We thanks prof. M.R. Groves and G. Kai for advice and help on MST assays.

Appendix A. Supplementary data

Supplementary data to this article can be found online at https://doi.org/10.1016/j.ejmech.2019.111849.

References

[1] B.R. Bloom, B. Bennett, Mechanism of a reaction in vitro associated with delayed hypersensitivity, Science 153 (1966) 80–82, https://doi.org/10.1126/science.153.3731.80.
[2] R. Bucala, Identification of MIF as a new pituitary hormone and macrophage cytokine and its role in endotoxic shock, Immunol. Lett. 43 (1994) 23–26, https://doi.org/10.1016/0165-2478(94)00152-9.
[3] O.A. Cherepkova, E.M. Lyutova, T.B. Eronina, B.Y. Gurvits, Chaperone-like activity of macrophage migration inhibitory factor, Int. J. Biochem. Cell Biol. 38 (2006) 43–55, https://doi.org/10.1016/j.biocel.2005.07.001.
[4] J. Bernhagen, R. Krohn, H. Lue, J.L. Gregory, A. Zernecke, R.R. Koenen, M. Dewor, I. Georgiev, A. Schober, L. Leng, T. Kooistra, G. Fingerle-Rowson, P. Ghezzi, R. Kleemann, S.R. McColl, R. Bucala, M.J. Hickey, C. Weber, MIF is a noncognate ligand of CXC chemokine receptors in inflammatory and atherogenic cell recruitment, Nat. Med. 13 (2007) 587–596, https://doi.org/10.1038/nm1567.
[5] T. Calandra, T. Roger, Macrophage migration inhibitory factor: a regulator of innate immunity, Nat. Rev. Immunol. 3 (2003) 791–800, https://doi.org/10.1038/nri1200.
[6] C.C.G. Nobre, J.M.G. de Araújo, T.A.A. de M. Fernandes, R.N.O. Cobucci, D.C.F. Lanza, V.S. Andrade, J.V. Fernandes, Macrophage migration inhibitory factor (MIF): biological activities and relation with cancer, Pathol. Oncol. Res. 23 (2017) 235–244, https://doi.org/10.1007/s12253-016-0138-6.
[7] L. Leng, C.N. Metz, Y. Fang, J. Xu, S. Donnelly, J. Baugh, T. Delohery, Y. Chen, R.A. Mitchell, R. Bucala, MIF signal transduction initiated by binding to CD74, J. Exp. Med. 197 (2003) 1467–1476, https://doi.org/10.1084/jem.20030286.
[8] X. Shi, L. Leng, T. Wang, W. Wang, X. Du, J. Li, C. Mcdonald, Z. Chen, J.W. Murphy, E. Lolis, P. Noble, W. Knudson, R. Bucala, N. Carolina, CD44 is the signaling component of the macrophage migration inhibitory factor-CD74 receptor complex, Immunity 25 (2006) 595–606, https://doi.org/10.1016/j.immuni.2006.08.020.
[9] R. Kleemann, A. Hausser, G. Geiger, R. Mischke, A. Burger-kentischer, O. Flieger, F. Johannes, T. Roger, T. Calandra, A. Kapurniotu, Intracellular action of the cytokine MIF to modulate AP-1 activity and the cell cycle through Jab1, Nature 408 (2000) 211–216, https://doi.org/10.1038/35041591.
[10] A.Y. Hoi, M.N. Iskander, E.F. Morand, Macrophage migration inhibitory factor: a therapeutic target across inflammatory diseases, Inflamm. Allergy - Drug

Targets 6 (2007) 183–190, https://doi.org/10.2174/187152807781696455.
[11] T. Calandra, B. Echtenacher, D.L. Roy, J. Pugin, C.N. Metz, L. Hültner, D. Heumann, D. Männel, R. Bucala, M.P. Glauser, Protection from septic shock by neutralization of macrophage migration inhibitory factor, Nat. Med. 6 (2000) 164–170, https://doi.org/10.1038/72262.
[12] C.M. Denkinger, M. Denkinger, J.J. Kort, C. Metz, T.G. Forsthuber, In vivo blockade of macrophage migration inhibitory factor ameliorates acute experimental autoimmune encephalomyelitis by impairing the homing of encephalitogenic T cells to the central nervous system, J. Immunol. 170 (2003) 1274–1282, https://doi.org/10.4049/jimmunol.170.3.1274.
[13] R.J. Kerschbaumer, M. Rieger, D. Völkel, D. Le Roy, T. Roger, J. Garbaraviciene, W.H. Boehncke, J. Müllberg, R.M. Hoet, C.R. Wood, G. Antoine, M. Thiele, H. Savidis-Dacho, M. Dockal, H. Ehrlich, T. Calandra, F. Scheiflinger, Neutralization of macrophage migration inhibitory factor (MIF) by fully human antibodies correlates with their specificity for the β-sheet structure of MIF, J. Biol. Chem. 287 (2012) 7446–7455, https://doi.org/10.1074/jbc.M111.329664.
[14] H. Ogawa, J. Nishihira, Y. Sato, M. Kondo, N. Takahashi, T. Oshima, S. Todo, An antibody for macrophage migration inhibitory factor suppresses tumour growth and inhibits tumour-associated angiogenesis, Cytokine 12 (2000) 309–314, https://doi.org/10.1006/cyto.1999.0562.
[15] K. Imai, A. Takaoka, Comparing antibody and small-molecule therapies for cancer, Nat. Rev. Cancer. 6 (2006) 714–727, https://doi.org/10.1038/nrc1913.
[16] P.G. Sasikumar, M. Ramachandra, Small - molecule immune checkpoint inhibitors targeting PD - 1/PD - L1 and other emerging checkpoint pathways, BioDrugs 32 (2018) 481–497, https://doi.org/10.1007/s40259-018-0303-4.
[17] Y. Al-Abed, D. Dabideen, B. Aljabari, A. Valster, D. Messmer, M. Ochani, M. Tanovic, K. Ochani, M. Bacher, F. Nicoletti, C. Metz, V.A. Pavlov, E.J. Miller, K.J. Tracey, ISO-1 binding to the tautomerase active site of MIF inhibits its pro-inflammatory activity and increases survival in severe sepsis, J. Biol. Chem. 280 (2005) 36541–36544, https://doi.org/10.1074/jbc.C500243200.
[18] J. Bloom, C. Metz, S. Nalawade, J. Casabar, K.F. Cheng, M. He, B. Sherry, T. Coleman, T. Forsthuber, Y. Al-Abed, Identification of iguratimod as an inhibitor of macrophage migration inhibitory factor (MIF) with steroid-sparing potential, J. Biol. Chem. 291 (2016) 26502–26514, https://doi.org/10.1074/jbc.M116.743328.
[19] Y. Zhang, L. Xu, Z. Zhang, Z. Zhang, L. Zheng, D. Li, Y. Li, F. Liu, K. Yu, T. Hou, X. Zhen, Structure – activity relationships and anti-inflammatory activities of N - carbamothioylformamide analogues as MIF tautomerase inhibitors, J. Chem. Inf. Model. 55 (2015) 1994–2004, https://doi.org/10.1021/acs.jcim.5b00445.
[20] H.W. Sun, J. Bernhagen, R. Bucala, E. Lolis, Crystal structure at 2.6-A resolution of human macrophage migration inhibitory factor, Proc. Natl. Acad. Sci. 93 (1996) 5191–5196, https://doi.org/10.1073/pnas.93.11.5191.
[21] J.B. Lubetsky, M. Swope, C. Dealwis, P. Blake, E. Lolis, Pro-1 of macrophage migration inhibitory factor functions as a catalytic base in the phenylpyruvate tautomerase activity, Biochemistry 38 (1999) 7346–7354, https://doi.org/10.1021/bi990306m.
[22] G. Pantouris, M.A. Syed, C. Fan, D. Rajasekaran, T.Y. Cho, E.M. Rosenberg, R. Bucala, V. Bhandari, E.J. Lolis, An analysis of MIF structural features that control functional activation of CD74, Chem. Biol. 22 (2015) 1197–1205, https://doi.org/10.1016/j.chembiol.2015.08.006.
[23] R. Kleemann, R. Mischke, A. Kapurniotu, H. Brunner, Specific reduction of insulin disulfides by macrophage migration inhibitory factor (MIF) with glutathione and dihydrolipoamide : potential role in cellular redox processes, FEBS Lett. 430 (1998) 191–196.
[24] H. Lue, H. Fu, R. Kleemann, P. Koolwijk, A. Kapurniotu, D. Tu, A 16-residue peptide fragment of macrophage migration inhibitory factor , MIF- (50 – 65), exhibits redox activity and has MIF-like biological functions, J. Biol. Chem. 278 (2003) 33654–33671, https://doi.org/10.1074/jbc.M301735200.
[25] V.C. Trivedi-Parmar, W.L. Jorgensen, Advances and insights for small molecule inhibition of macrophage migration inhibitory factor, J. Med. Chem. 61 (2018) 8104–8119, https://doi.org/10.1021/acs.jmedchem.8b00589.
[26] T. Kok, A.A. Wasiel, R.H. Cool, B.N. Melgert, G.J. Poelarends, F.J. Dekker, Small-molecule inhibitors of macrophage migration inhibitory factor (MIF) as an emerging class of therapeutics for immune disorders, Drug Discov. Today 23 (2018) 1910–1918, https://doi.org/10.1016/j.drudis.2018.06.017.
[27] L. Xu, Y. Li, H. Sun, X. Zhen, C. Qiao, S. Tian, T. Hou, Current developments of macrophage migration inhibitory factor (MIF) inhibitors, Drug Discov, Today 18 (2013) 592–600, https://doi.org/10.1016/j.drudis.2012.12.013.
[28] J.B. Lubetsky, A. Dios, J. Han, B. Aljabari, B. Ruzsicska, R. Mitchell, E. Lolis, Y. Al-Abed, The tautomerase active site of macrophage migration inhibitory factor is a potential target for discovery of novel anti-inflammatory agents, J. Biol. Chem. 277 (2002) 24976–24982, https://doi.org/10.1074/jbc.M203220200.
[29] M. Orita, S. Yamamoto, N. Katayama, M. Aoki, K. Takayama, Y. Yamagiwa, N. Seki, H. Suzuki, H. Kurihara, H. Sakashita, M. Takeuchi, S. Fujita, T. Yamada, A. Tanaka, Coumarin and chromen-4-one analogues as tautomerase inhibitors of macrophage migration inhibitory factor: discovery and X-ray crystallography, J. Med. Chem. 44 (2001) 540–547, https://doi.org/10.1021/jm000386o.
[30] T. Kok, H. Wapenaar, K. Wang, C.G. Neochoritis, T. Zarganes-Tzitzikas, G. Proietti, N. Eleftheriadis, K. Kurpiewska, J. Kalinowska-Tłuścik, R.H. Cool, G.J. Poelarends, A. Dömling, F.J. Dekker, Discovery of chromenes as inhibitors of macrophage migration inhibitory factor, Bioorg. Med. Chem. 26 (2018) 999–1005, https://doi.org/10.1016/j.bmc.2017.12.032.
[31] L. Xu, Y. Zhang, L. Zheng, C. Qiao, Y. Li, D. Li, X. Zhen, T. Hou, Discovery of novel inhibitors targeting the macrophage migration inhibitory factor via structure-based virtual screening and bioassays, J. Med. Chem. 57 (2014) 3737–3745, https://doi.org/10.1021/jm401908w.
[32] J.A. Cisneros, M.J. Robertson, M. Valhondo, W.L. Jorgensen, A fluorescence polarization assay for binding to macrophage migration inhibitory factor and crystal structures for complexes of two potent inhibitors, J. Am. Chem. Soc. 138 (2016) 8630–8638, https://doi.org/10.1021/jacs.6b04910.
[33] W.L. Jorgensen, S. Gandavadi, X. Du, A.A. Hare, A. Trofimov, L. Leng, R. Bucala, Receptor agonists of macrophage migration inhibitory factor, Bioorg. Med. Chem. Lett 20 (2010) 7033–7036, https://doi.org/10.1016/j.bmcl.2010.09.118.
[34] P. Dziedzic, J.A. Cisneros, M.J. Robertson, A.A. Hare, N.E. Danford, R.H.G. Baxter, W.L. Jorgensen, Design, synthesis, and protein crystallography of biaryltriazoles as potent tautomerase inhibitors of macrophage migration inhibitory factor, J. Am. Chem. Soc. 137 (2015) 2996–3003, https://doi.org/10.1021/ja512112j.
[35] T.K. Dawson, P. Dziedzic, M.J. Robertson, J.A. Cisneros, S.G. Krimmer, A.S. Newton, J. Tirado-Rives, W.L. Jorgensen, Adding a hydrogen bond may not help: naphthyridinone vs quinoline inhibitors of macrophage migration inhibitory factor, ACS Med. Chem. Lett. 8 (2017) 1287–1291, https://doi.org/10.1021/acsmedchemlett.7b00384.
[36] J.A. Cisneros, M.J. Robertson, M. Valhondo, W.L. Jorgensen, Irregularities in enzyme assays: the case of macrophage migration inhibitory factor, Bioorg. Med. Chem. Lett 26 (2016) 2764–2767, https://doi.org/10.1016/j.bmcl.2016.04.074.
[37] C. Guo, M. Saifuddin, T. Saravanan, G.J. Poelarends, Biocatalytic asymmetric Michael additions of nitromethane to α , β - unsaturated aldehydes via enzyme-bound iminium ion intermediates, ACS Catal. 9 (2019) 4369–4373, https://doi.org/10.1021/acscatal.9b00780.
[38] V.A. Kostevich, A.V. Sokolov, N.A. Grudinina, E.T. Zakharova, V.R. Samygina, V.B. Vasilyev, Interaction of macrophage migration inhibitory factor with ceruloplasmin: role of labile copper ions, Biometals 28 (2015) 817–826, https://doi.org/10.1007/s10534-015-9868-2.
[39] G.V. Crichlow, F.C. Kai, D. Dabideen, M. Ochani, B. Aljabari, V.A. Pavlov, E.J. Miller, E. Lolis, Y. Al-Abed, Alternative chemical modifications reverse the binding orientation of a pharmacophore scaffold in the active site of macrophage migration inhibitory factor, J. Biol. Chem. 282 (2007) 23089–23095, https://doi.org/10.1074/jbc.M701825200.
[40] P.M.G. Finn, V. Fokin, J.E. Hein, V.V. Fokin, Copper-catalyzed azide–alkyne cycloaddition (CuAAC) and beyond: new reactivity of copper(I) acetylides, Chem. Soc. Rev. 39 (2010) 1302–1315, https://doi.org/10.1039/b904091a.
[41] Y.-C. Cheng, W.H. Prusoff, Relationship between the inhibition constant (Ki) and the concentration of inhibitor which causes 50 percent inhibition (I50) of an enzymatic reaction, Biochem. Pharmacol. 22 (1973) 3099–3108, https://doi.org/10.1016/0006-2952(73)90196-2.
[42] P. Dziedzic, J.A.J.A. Cisneros, M.J. Robertson, A.A. Hare, N.E. Danford, R.H.G.G. Baxter, W.L. Jorgensen, E. Nadia, R.H.G.G. Baxter, W.L. Jorgensen, Design, synthesis, and protein crystallography of biaryltriazoles as potent tautomerase inhibitors of macrophage migration inhibitory factor. SI, J. Am. Chem. Soc. 137 (2015) 2996–3003, https://doi.org/10.1021/ja512112j.
[43] C.J. Wienken, P. Baaske, U. Rothbauer, D. Braun, S. Duhr, Protein-binding assays in biological liquids using microscale thermophoresis, Nat. Commun. 1 (2010) 1–7, https://doi.org/10.1038/ncomms1093.
[44] B.E. Rendon, T. Roger, I. Teneng, M. Zhao, Y. Al-abed, T. Calandra, R.A. Mitchell, Regulation of human lung adenocarcinoma cell migration and invasion by macrophage migration inhibitory factor, J. Biol. Chem. 282 (2007) 29910–29918, https://doi.org/10.1074/jbc.M704898200.
[45] M. Le Hiress, B. Akagah, G. Bernadat, L. Tu, A. Huertas, C. Phan, E. Fadel, M. Humbert, C. Guignabert, Design, synthesis, and biological activity of new N - (phenylmethyl)- benzoxazol-2-thiones as macrophage migration inhibitory factor (MIF) antagonists: Efficacies in experimental pulmonary hypertension, J. Med. Chem. 61 (2018) 2725–2736, https://doi.org/10.1021/acs.jmedchem.7b01312.
[46] J. Bernhagen, R.A. Mitchell, T. Calandra, W. Voelter, A. Cerami, R. Bucala, Purification, bioactivity, and secondary structure analysis of mouse and human macrophage migration inhibitory factor (MIF), Biochemistry 33 (1994) 14144–14155, https://doi.org/10.1021/bi00251a025.